Title
Quantitative MRI of articular cartilage and its clinical applications

Journal
Journal of Magnetic Resonance Imaging, 38(5)

ISSN
1053-1807

Authors
Li, Xiaojuan
Majumdar, Sharmila

Publication Date
2013-11-01

DOI
10.1002/jmri.24313

Peer reviewed

Published in final edited form as:
J Magn Reson Imaging. 2013 November ; 38(5): . doi:10.1002/jmri.24313.

QUANTITATIVE MAGNETIC RESONANCE IMAGING OF ARTICULAR CARTILAGE AND ITS CLINICAL APPLICATIONS

Xiaojuan Li, Ph.D.[*] and **Sharmila Majumdar, Ph.D.**
Musculoskeletal Quantitative Imaging Research Group, Department of Radiology and Biomedical Imaging, University of California, San Francisco, CA, USA

Abstract

Cartilage is one of the most essential tissues for healthy joint function and is compromised in degenerative and traumatic joint diseases. There have been tremendous advances during the past decade using quantitative MRI techniques as a non-invasive tool for evaluating cartilage, with a focus on assessing cartilage degeneration during osteoarthritis (OA). In this review, after a brief overview of cartilage composition and degeneration, we discuss techniques that grade and quantify morphologic changes as well as the techniques that quantify changes in the extracellular matrix. The basic principles, *in vivo* applications, advantages and challenges for each technique are discussed. Recent studies using the OA Initiative (OAI) data are also summarized. Quantitative MRI provides non-invasive measures of cartilage degeneration at the earliest stages of joint degeneration, which is essential for efforts towards prevention and early intervention in OA.

Keywords

Osteoarthritis; Cartilage; Quantitative MRI

CARTILAGE COMPOSITION AND DEGENERATION

Hyaline cartilage consists of a low density of chondrocytes and a large extracellular matrix (ECM) (1). The ECM is composed primarily of water (~75% of cartilage by weight), and a cross-linked matrix with proteoglycans (PG) and type-II collagen fibers. The GAG is highly negatively charged. A key function of these aggregates is to provide a stable environment of high fixed-charge density (FCD), essential for imbibing and retaining water in the tissue by the high osmotic swelling pressure created. The distribution and orientation of collagen in cartilage demonstrates anatomical zones at microscopy. The collagen fibers are oriented parallel to the articular surface in the superficial zone (10% ~ 20%), arcade like in the transitional zone (40% ~ 60%), and perpendicular in the radial zone (30% ~ 40%). The superficial zone can be further divided into two sub-zones: the lamina splenden, the more superficial layer with dense small fibrils and little polysaccharide and no cells; and the cellular layer with flattened chondrocytes and collagen fibers tangentially to the articular surface (http://www.wheelessonline.com/ortho/articular_cartilage). Below radial zone is a thin layer of calcified cartilage, separated by the tidemark. Although the etiopathogenesis of OA is not fully understood, it is believed that OA results from an imbalance between predominantly chondrocyte-controlled anabolic and catabolic processes, and is characterized by progressive degradation of the components of cartilage ECM (2). Changes at early stages of OA include hydration, PG loss, thinning and disruption of collagen, although it has been

[*]Corresponding Author: Xiaojuan Li, PhD, 185 Berry St, Suite 350, San Francisco, CA 94107, Tel: 415-353-4909, Fax: 415-353-9423, xiaojuan.li@ucsf.edu, Sharmila Majumdar, Ph.D. QB3 Building, 2nd Floor, Suite 203, 1700 - 4th Street, San Francisco, CA 94158, Tel: 415-476-6830, Fax: 415-514-9656, sharmila.majumdar@ucsf.edu.

suggested neither the content nor the type of collagen is altered at early stages (1). Changes in late stages include dehydration, resulting in extensive fibrillation and loss of the cartilage and eventually denudation of the subchondral bone. Fig. 1 illustrates the different stages of cartilage degeneration.

MORPHOLOGICAL CHANGES IN CARTILAGE IN OSTEOARTHRITIS

Magnetic resonance provides excellent soft tissue contrast and clinical evaluation of articular cartilage is normally based on proton density or intermediate-weighted fast spin-echo images. Both fat suppressed and non-fat suppressed images have been used. Fat-suppressed images provide better contrast between cartilage and surrounding tissues, while non-fat suppressed images permits higher spatial resolution without the loss of signal to noise afforded by routine fat suppression. Normally, a wider receiver bandwidth will be used in non-fat suppressed imaging to reduce chemical shift artifact at the cartilage-subcondral bone interface. Morphological grading of the cartilage is to quantify cartilage changes in OA have also been developed. The Whole Organ Magnetic Resonance Imaging Score (WORMS) of the knee in OA was proposed by Peterfy et al. (3) and is one that characterizes multiple features in cartilage, meniscus, ligaments, bone marrow, all believed to be relevant to the pathophysiology of OA. Fig. 2 shows representative MR images with corresponding WORMS scores. The Boston-Leeds OA Knee Score or the BLOKS score (4) focuses on bone marrow edema like lesions and has been related to pain in OA.

Apart from the grading systems, high resolution typically fat-suppressed MR images have also been used to quantify cartilage thickness and volume. Apart from compartmental analysis (ie medial vs lateral compartment), sub-regional analysis of cartilage volume and thickness has been undertaken especially by Eckstein et al. (5). Pulse sequences that are used to obtain images for cartilage volume estimation have high signal-to-noise ratio, high contrast-to-noise ratio and high resolution as the cartilage thickness of a few mm warrants that the image resolution be as high as possible. Three-dimensional spoiled gradient echo images (SPGR) and a number of variants on these sequences such as dual echo steady state (DESS) images with different methods of fat suppression as well as newly developed 3D fast spin-echo images have been used for the assessment of cartilage morphology.

The steps involved in assessing cartilage volume and thickness include the segmentation of the cartilage. Several different image processing approaches have been proposed for this purpose. Stammberger and colleagues (6) applied a quadratic B-spline to guide the segmentation. An internal energy term controlled the rigidity of the contour, an external energy term attracted the contour to the cartilage edges, and a coupling force enforced smooth changes from one slice to another. In another 2D approach, Lynch et al. (7) combined expert knowledge with cubic splines and image processing algorithms reporting better reproducibility and less user interaction than region growing techniques. Grau et al. (8) extended the watershed technique to examining difference in class probability of neighboring pixels. Pakin et al. (9) used a region growing method with prior knowledge. Warfield and colleagues (10) developed an adaptive, template moderated, spatially varying statistical classification method, which consisted of an iterative technique between classification and template registration. Manual editing is often required in the context of semi-automated cartilage segmentation. After segmentation, the simplest morphological measure to compute is the sum of the total number of voxels representing cartilage, followed by corresponding scaling according to the voxel dimensions. The most common approach to compute cartilage thickness is based on 2D or 3D minimum Euclidean distances (11). For each point on the bone-cartilage interface or articular surface, the closest point on the opposite surface is computed. Another 3D approach consists on computing normal vectors on one surface (articular or bone-cartilage interface), and finding the intersection of the

vectors on the opposite surface (12). The average of the minimum distances or length of the vectors, respectively, is reported as the average cartilage thickness. Fig. 3 shows a thickness map of the knee cartilage.

To obtain a measure of the spatial distribution of change (between time points) in cartilage volume and thickness, image registration is required. For this purpose some investigators have used the bone-cartilage interface (13) while others have used the total bone shape (14). Once shapes have been aligned, matching of cartilage thickness patterns can be performed at a local level. Because there is an increasing interest in performing regional comparisons of cartilage properties at specific anatomic locations between different populations for a better understanding of OA, techniques have also been developed for this purpose (11, 15). For inter-subject comparisons, shapes have to be registered prior to any comparison, but in this case, scale factors as well as nonlinear differences between shapes have to be considered. The bone shape, and not only the interface, has recently been proposed for this type of matching (11). Fig. 4 shows an intra-subject longitudinal example of cartilage thickness matching using the technique described by Carballido-Gamio and colleagues, which can also be applied for inter-subject comparisons of cartilage properties (11).

Quantitative Morphology in the OAI

The OA Initiative – OAI (http://oai.epi-ucsf.org/datarelease/StudyOverview.asp) is a multi-center, longitudinal, prospective observational study of knee OA. The aim of the OAI is to develop a public domain research resource to facilitate the scientific evaluation of biomarkers for OA as potential surrogate endpoints for disease onset and progression. The OAI data includes clinical evaluation data, imaging (x-ray and 3 Tesla MR), and a biospecimen repository from 4796 men and women ages 45–79 years. The participants include those who are at high risk for developing, symptomatic knee OA. Using the MR data from these studies investigators have determined that the MR sequences used to estimate the cartilage thickness and volume have adequate reproducibility. Rates of change for cartilage morphological measures in different regions have been proposed as a function of radiographic disease extent, existence of pain, and predictor of knee replacement, which has been recently reviewed by Eckstein et al (16).

QUANTITATIVE MRI FOR CARTILAGE MATRIX COMPOSITION

As discussed previously, cartilage degeneration starts with changes in hydration and the macromolecular structures, specifically PG and collagen network, within the matrix. Techniques that are sensitive and specific to these changes are ideal for early detection of cartilage degeneration. Water content in cartilage has been quantified by using proton density images after corrections of T_1 and T_2 relaxation values, which however has limited sensitivity of detecting early cartilage degeneration due to the relatively small changes of water contents in osteoarthritic cartilage (up to 9%) (17). Current efforts have been made more towards measuring the changes associated with marcomolecular changes, PG and collagen, within the matrix. However, both PG and collagen protons sustain very short T_2 relaxation time due to their macromolecular structures, and it is difficult to measure them directly with MRI, except for using *ex vivo* high field NMR techniques. As a result, current MRI techniques are primarily focused on sensitizing the measurement of water proton signals to the macromolecular contents and structures in the matrix based on energy and magnetization exchange between bulk-water protons and protons associated with macromolecules. We classified the quantitative MRI methods for cartilage matrix biochemistry into four categories: 1) methods based on relaxometry including T_1 (with and without presence of contrast agent), T_2 and $T_{1\rho}$ relaxation time quantification; 2) methods based on diffusion measurement; 3) methods based on magnetization transfer measurement including conventional magnetization transfer and chemical exchange saturation transfer

(CEST); and 4) a non-proton method, sodium imaging, has been developed and applied to measure cartilage matrix changes, which will be also discussed in this review.

Post-Contrast T_1 Relaxation Time by Delayed Gadolinium-Enhanced Proton MRI of Cartilage

Basic Principles—As T_1 reflects activities with relaxation correlation time in the range of $1/(\gamma B_0)$, native T_1 measurement is normally not sensitive to cartilage matrix changes due to the slow motion of the restricted protons in the matrix. However, delayed gadolinium (Gd)-enhanced proton MRI of cartilage (dGEMRIC) has been developed to quantify PG content in cartilage by quantifying T_1 with the presence of the contrast agent (18, 19). It is based on the fact that PG, or the associated GAG, has abundant negatively charged carboxyl and sulfate groups. In the study of dGEMRIC, contrast agent of gadolinium diethylene triamine pentaacetic acid, or Gd-DTPA^{2-} (Magnevist; Berlex Laboratories, Wayne, NJ), is injected intravenously (or intra-articularly) and distributed in the cartilage by diffusion. The diffusion time depends on the cartilage thickness and is approximately two hours in femoral weight-bearing cartilage. Because Gd-DTPA^{2-} is negatively charged, it will be distributed in a relatively low concentration in areas that are rich in GAG (normal cartilage), and in higher concentrations in regions with depleted GAG (degenerated cartilage). Gd-DTPA^{2-} has a concentration-dependent effect on the MR parameter T_1. Therefore T_1-weighted images in the presence of Gd-DTPA^{2-} reflect the Gd-DTPA^{2-} concentration, and hence tissue GAG concentration. By calculating T_1 relaxation time, the concentration of GAG can be quantified based on a modified electrochemical equilibrium theory, assuming the Gd-DTPA^{2-} is equilibrated in the tissue (18).

dGEMRIC measures have been validated using biochemical and histologic measurements of GAG concentration in cartilage with *ex vivo* studies, as reviewed by Gray et al. (19). The *in vivo* validation of dGEMRIC techniques, however, was not straightforward especially for the conversion from T_1 quantification to GAG concentration, therefore the direct T_1 measures of ‘dGEMRIC index’ was normally reported for clinical studies (19). Loss of GAG will result in a decreased T1, and a decreased ‘dGEMRIC index’.

In vivo applications—The sequences for *in vivo* T_1 quantification in dGEMRIC studies include the most commonly used two-dimensional (2D) inversion recovery fast spin-echo (IR-FSE) sequences due to its widespread availability of the sequence and desirable contrast properties (cartilage versus fluid), 3D acquisitions based on IR-spoiled gradient echo (IR-SPGR) for better coverage, and fast 3D methods based on Look-Locker or based on spoiled GRE images with two optimized flip angles. Good correlations were reported between measures from the 3D methods and the gold-standard 2D IR-FSE technique. The reproducibility of the 3D-variable flip angle method (RMS-CV: 9.3–15.2%) was reported to be inferior compared to 2D-IR FSE and 3D Look Locker methods (RMS-CV: 5.8–8.4%) (20). In particular, the investigators suggested that positioning of the analyzed images is crucial to generate reliable repeatability results. The recommended clinical protocol was summarized by Burstein et al. (21).

Decreased dGEMRIC index was observed in compartment with radiography joint space narrowing compared to other compartment (22). In obese subjects, knee dGEMRIC index was associated with age, clinical knee OA, abnormal tibiofemoral alignment, and quadriceps strength (23). Subjects with medial meniscectomy (1–6 years before imaging) showed significantly lower dGEMRIC Index of the medial compartment after surgery (24). In subjects with acute anterior cruciate ligament (ACL) injuries, significantly decreased dGEMRIC index was observed in ACL-injured knees compared to either contralateral knees or knees from healthy control subjects (25, 26), suggesting that dGEMRIC index may be

indicative of potential early degeneration in knees with risk of developing post-traumatic OA.

In the hip, lower dGEMRIC index was reported in subjects with femoroacetabular impingement (FAI) with different patterns of subregional variation between subjects with cam and pincer FAI (27), and was correlated with the magnitude of the deformity and pain (28). In subjects with hip dysplasia, a developmental malformation of the hip associated with early OA, Kim et al. reported that dGEMRIC significantly correlated with severity of dysplasia and pain (29), Fig. 5.

Advantages and Challenges—Previous studies support the dGEMRIC index as a clinically relevant measure of cartilage integrity, with specific measures related to GAG concentration. However, one should be aware that especially for *in vivo* studies, bias may be introduced during conversion from dGEMRIC measures to GAG concentration due to factors such as the possibility of altered contrast agent relaxivity under different tissue conditions and other factors such as the transport of contrast agent into cartilage with a variable blood concentration that might affect the equilibrating concentration of $Gd(DTPA)^{2-}$ in vivo (19). Other challenges that hinder dGEMRIC from widespread clinical application including necessity of contrast agent injection, and long delay of MR scan after Gd injection.

T_2 Relaxation Time

Basic Principles—T_2 relaxation time, or the spin-spin relaxation time, reflects the ability of free water proton molecules to move and to exchange energy inside the cartilaginous matrix. It has been shown that in normal cartilage this transverse (T_2) relaxation is dominated by the anisotropic motion of water molecules in a fibrous collagen network. Damage to collagen-PG matrix and increase of water content in degenerating cartilage may increase T_2 relaxation times.

T_2 quantification is normally performed by fitting T_2-weighted images acquired with different TEs to mono- or multi-exponential decay curve. Pai et al. compared the T_2 mapping techniques in phantoms and *in vivo* based on five different sequences with regard to SNR, reproducibility and quantification: spin-echo (SE), fast spin-echo (FSE), multi-echo SE (MESE), magnetization prepared 2D spiral, and magnetization prepared 3D SPGR (30). Variation of T_2 quantification was observed, Fig. 6, which may due to different sensitivity of each sequences to system imperfections including stimulated echoes, off resonance signals and eddy currents. Different fitting methods will also introduce bias to T_2 quantification. Caution needs to be exercised when comparing results from different studies and when designing a multi-center study.

In vitro studies have reported that T_2 correlated with water content but poorly with PG depletion in enzymatically degraded articular cartilage (31). Using high field microscopic MRI (μMRI), Xia et al. showed that T_2 spatial variation is dominated by the ultra-structure of collagen fibrils, and thus angular dependency of T_2 with respect to the external magnetic field B_0 can provide specific information about the collagen structure (32). T_2 variation was also correlated with polarized light microscopy (33). This angular dependency of T_2, results in the ‘magic angle’ effect and commonly seen laminar appearance in cartilage imaging. Multi-exponential T_2 relaxation components were identified by Reiter et al. using intact and enzyme digested bovine nasal cartilage (34). Using bovine nasal cartilage, it was demonstrated that this multi-component properties may depend on the orientation of collagen fibers with respect to B_0 – at the magic angle (55°), T_2 (and $T_{1\rho}$) were a single component rather than multiple-components (35). This multiexponential approach has the

potential to improve specificity of cartilage matrix evaluation using T_2 relaxation parameters.

In vivo Applications—*In vivo* T_2 values have been shown to vary from the subchondral bone to the cartilage surface (36, 37). With the exception of the lamina splendens, T_2 decreased from the superficial layer to the deep layer. Cartilage T_2 has been correlate with age (38), but not with gender (39). Elevated T_2 relaxation times were observed in OA cartilage, and were associated with the severity of disease categorized with radiography (40). In one study examining T_2 in patellar cartilage, however, no differences of T_2 values were found across the stages of OA based on radiographic KL scores ($P = 0.25$) (41). The same study reported increased T_2 was associated with increased BMI, suggesting BMI is a significant factor for increasing T_2. Increase of T_2 (and $T_{1\rho}$) was also correlated with decreased trabecular bone structure in OA knees, highlighting the interplay between cartilage and bone structure in OA (42, 43).

T_2 quantification has been used as non-invasive measures to quantify and monitor the change in biochemical and biomechanical properties of cartilage after physical activity or exercise. Mosher et al. reported that cartilage T_2 values decreased after running, along with a decrease in cartilage thickness (44), suggested the decrease of water contents and changes of collagen network after high impact activity such as running. A more recent study showed the greatest decrease of T_2 and $T_{1\rho}$ after running occurred in the superficial layer of medial femoro-tibial and patella-femoral cartilage (45), suggesting greater load sharing by these areas during running. Further studies in subjects with OA would be interesting to examine the loading pattern and cartilage response to running in degenerative joints.

T2 quantification has been also applied in evaluating early cartilage matrix changes after acute injuries, such as acute anterior cruciate (ACL) tears. In a very recent longitudinal study, Potter et al. reported that T2 values were elevated during follow-ups (up to 11 years after injury) in the lateral side and patella after isolated ACL tears (T2 values in the medial side were not available), indicating accelerated cartilage degradation in such joints (46). The T2 elevation was observed in regions that were not covered by the intial bone marrow edema-like lesions, suggesting the injury initiated a rather global disturbing of cartilage homeostasis within the whole joint.

In vivo T_2 quantification using a multi-slice multi-echo spin-echo (MESE) sequence has been included in the OA Initiative. Data from the monthly quality assurance procedure over a 3-year period showed excellent longitudinal reproducibility (RMS CV < 5%) except for one site (47). Cartilage T_2 values have been correlated to physical activity levels (determined by Physical Activity Scale for the Elderly), in particular knee bending activities, in OAI cohort (48). Light exercisers had lower T_2 values compared with both sedentary and moderate/strenuous exercisers in subjects with risk factors for knee OA (n = 128), Fig. 7, suggesting that there could be a “U” shape of the effect of exercise to cartilage biochemistry – either too little or too much will be detrimental, but the optimized appropriate level of exercise for each individual may be affected by many factors including BMI, genetic profile, biomechanical characteristics such as alignment and kinematics. Nonetheless, as exercise is a modified factor, exploring the relationship of different type and level of exercise to cartilage biochemistry as quantified by advanced MRI can be clinically valuable to allow intervention and training to prevent and slow down cartilage degeneration.

Using OAI data, a 2-year longitudinal analysis of OAI normal cohort showed a significant increase in T_2 was in the tibiofemoral cartilage while no changes in the patellofemoral cartilage (49). A greater increase in cartilage T_2 was found to correlate with an increase in the progression of cartilage abnormalities (graded with WORMS). More recently, Joseph et

al. reported, in OAI subjects with risk factors for OA (n = 289), the baseline mean and heterogeneity of cartilage T_2 were significantly ($P<0.05$) associated with morphologic joint degeneration in the cartilage, meniscus and bone marrow over 3 years (50). These studies suggested that characterizing and monitoring the cartilage matrix integrity with T_2 measurements might enable identification of individuals at risk for the development of early OA before irreversible cartilage loss occurs.

Advantages and Challenges—Cartilage T_2 quantification is a promising marker for cartilage matrix biochemistry and has been applied in the largest multi-center studies of OA with the effort of the OAI. T_2 changes are dominated by the hydration and collagen fibers and may not be sensitive to subtle changes of PG loss. Caution is also needed during data interpretation due to the magic angle effect of T_2. In addition, due to the layer variation of cartilage T_2 as discussed earlier, laminar analysis is recommended to be used for analyzing either OA or cartilage repair data. It should be noted that sampling quantitative data in the superficial zone or lamina splendens is technically challenging, and normally two layers (with equal thickness) were used for in vivo T2 laminar analysis due to the limited resolution of in vivo T2 mapping.

$T_{1\rho}$ Relaxation Time Quantification

Basic Principles—The $T_{1\rho}$ parameter is defined as the time constant describing the spin-lattice relaxation in the rotating frame. It probes the slow motion interactions between motion- restricted water molecules and their local macromolecular environment. The macromolecules in articular cartilage ECM restrict the motion of water molecules. Changes to the ECM, such as PG loss, therefore, can be reflected in measurements of $T_{1\rho}$ The $T_{1\rho}$ is normally measured by the spin-lock (SL) technique, which enabled study of relaxation at very low field without sacrificing the SNR afforded by higher field strengths. In an SL experiment, spins are flipped into the transverse plane along one axis, immediately followed by a SL pulse applied along the same axis. A SL pulse is an on-resonance, continuous wave radiofrequency (RF) pulse, normally long-duration and low-energy. Since the magnetization and RF field are along the same direction, the magnetization is “spin-locked” provided the locking condition is satisfied, i.e., the B_1 of locking pulses is much stronger than the local magnetic fields generated by, for example, magnetic moments of nuclei. The spins will relax with a time constant $T_{1\rho}$ along B_1 of locking pulses in the transverse plane. The amplitude of the SL pulse is commonly referenced in terms of the nutation frequency ($f = \gamma B_1$). The normal range of SL frequency is a few hundreds hertz to a few kilohertz. $T_{1\rho}$ relaxation phenomena are sensitive to physicochemical processes with inverse correlation times on the order of the nutation frequency of the SL pulse. $T_{1\rho}$ increases as the strength of the SL field increases, a phenomenon termed $T_{1\rho}$ dispersion. $T_{1\rho}$ dispersions may also have tissue specificity.

The $T_{1\rho}$ -weighted imaging sequences are composed of two parts: magnetization preparation with $T_{1\rho}$ weighting using spin-lock pulse cluster, and a following 2D (based on spiral, or fast spin-echo or echo planar imaging) or 3D (based on gradient echo or 3D fast spin echo) data acquisition. Compared to 2D acquisition, 3D sequences have the advantage of higher image resolution, especially in the slice direction. Among 3D sequences, the method using transient signals immediately after $T_{1\rho}$ preparation either based on SPGR acquisition (51) (magnetization-prepared angle-modulated partitioned k-space spoiled gradient echo snapshots, MAPSS) or based on balanced GRE acquisition (52) are more SNR efficient and less SAR intensive compared to the method based on the steady state GRE acquisition (53). These sequences have been implemented at both 1.5T and 3T on scanners from different manufactures. Several modifications in the SL pulse cluster and phase cycling were

performed in order to improve the robustness of spin locking to B_0 and B_1 inhomogeneity (54, 55).

In vitro studies have showed that the elevation of $T_{1\rho}$ relaxation time was correlated with PG loss in both bovine (31) and human cartilage (56), and with histological grading (56). In $T_{1\rho}$ quantification experiments, the spin-lock techniques reduce dipolar interactions and therefore reduce the dependence of the relaxation time constant on collagen fiber orientation. This enables more sensitive and specific detection of changes in PG content using $T_{1\rho}$ quantification, although $T_{1\rho}$ changes in cartilage may be affected by hydration and collagen structure as well. The reduced dipolar interaction also results in less 'magic angle effect' in $T_{1\rho}$ imaging as compared to T_2 imaging. Less laminar appearance was observed in $T_{1\rho}$ -weighted images compared to T_2-weighted images (57). Previous specimen studies reported that $T_{1\rho}$ values at the magic angle (54.7°) were significantly higher than at other angles, but the difference was smaller than the different in T_2 values at the same angles (56). The different was decreased with increased $T_{1\rho}$ spin-lock frequencies and was diminished when $T_{1\rho}$ spin-lock frequency was equal to or higher than 2K Hz (57).

Previous studies suggested that proton exchange between NH and OH groups of GAG and bulk water contribute significantly to the $T_{1\rho}$ relaxation (58), while another study suggested that the contribution of scalar relaxation caused by proton exchange is only relevant at high fields such as 7T (59). Other evidence of a proton exchange pathway is the PH dependency of $T_{1\rho}$ values in the ischemic rat brain tissues (60). Further investigations are needed to better understand this relaxation mechanism in cartilage.

In vivo Applications—*In vivo* $T_{1\rho}$ reproducibility (scan-rescan studies at a single center) was reported to range from 1.7% - 8.7% (51). A recent multicenter study reported reproducibility CVs for both T_2 (4–14%) and $T_{1\rho}$ (7–19%) (61). Future studies are warranted to evaluate multi-site multi-vendor variation of $T_{1\rho}$ and T_2 quantification with a clinical trial setup. *In vivo* studies suggested $T_{1\rho}$ is moderately age-dependent (62). Increased cartilage $T_{1\rho}$ values was observed in OA subjects compared to controls (40, 42, 53, 62) in asymptomatic active healthy subjects with focal cartilage abnormalities compared to those without lesions (62), in subjects with meniscal tears compared to those without tears (63), and in regions overlying bone marrow edema-like lesions (BMEL) compared to surrounding cartilage in OA and acutely-injured knees (64). Further, elevated $T_{1\rho}$ was observed in subcompartments in OA subjects where no obvious morphologic changes were observed, suggesting the capability of $T_{1\rho}$ in detecting very early biochemical changes within the cartilage matrix (40).

Similar as T_2, $T_{1\rho}$ values decreased from the superficial zone (excluding the lamina splendens) to the deep zone of cartilage (37). Although the trend of $T_{1\rho}$ and T_2 values are similar, $T_{1\rho}$ shows a larger dynamic range and less laminar appearance was observed in $T_{1\rho}$ -weighted images compared to T_2-weighted images due to reduced dipolar interaction during $T_{1\rho}$ relaxation (57). In human subjects, the pixel-by-pixel correlation between $T_{1\rho}$ and T_2 was reported to have a large range in both controls and OA patients ($R^2 = 0.522 \pm 0.183$, ranging from 0.221 to 0.763 in OA patients vs. $R^2 = 0.624 \pm 0.060$, ranging from 0.547 to 0.726 in controls) (37). Fig. 8 shows $T_{1\rho}$ and T_2 maps from a control subject, a subject with mild OA, and a subject with severe OA. The differences between the $T_{1\rho}$ and T_2 maps are evident. These results suggested $T_{1\rho}$ and T_2 show different spatial distribution and may provide complementary information regarding cartilage degeneration in OA. Combining these two parameters may further improve our capability to diagnose early cartilage degeneration and injury.

In addition to patients with OA, $T_{1\rho}$ quantification techniques have been applied to patients with acutely injured knees, who have a high risk of developing OA later in life. In patients with acute ACL tears, significantly increased $T_{1\rho}$ values were found at baseline (after injury but prior to ACL reconstruction) in cartilage overlying bone marrow edema-like lesions (BMEL) when compared with surrounding cartilage at the lateral tibia (64). Follow up exams at one-year after ACL-reconstruction of these ACL injured knees (65) showed that 1) in lateral sides, despite the resolution of BMEL, cartilage overlying the baseline BMEL still show significantly higher $T_{1\rho}$ compared to the surrounding cartilage, suggesting potential irreversible damage of cartilage in these regions; 2) in medial sides, $T_{1\rho}$ values in medial tibial and medial femoral condyles, especially the contact area (the contact area during supine unloaded MRI), show significant elevation at as early as one-year after ACL reconstruction compared to healthy controls, probably due to abnormal kinematics even after ACL reconstruction, Fig. 9. T_2 also showed increasing trend in these regions of cartilage, however it did not reach statistical significance. The authors speculated that $T_{1\rho}$ is more sensitive than T_2 in detecting cartilage damages and potential early degeneration in ACL-injured knees (65). It should be noted that at the spin-lock frequencies that are commonly used for in vivo studies (400 Hz – 500 Hz), $T_{1\rho}$ quantification also showed orientation dependency as discussed earlier. Therefore, $T_{1\rho}$ values of subregions along the femoral condyles cannot be compared directly. Rather, the values should be compared to match-regions in control knees. To increase the spin-lock frequency will decrease the orientation dependency, but the highest spin-lock frequency will be limited by the energy deposited to the tissue as evaluated by specific absorption rate (SAR) or by the maximum B1 allowed by the hardware.

Advantages and Challenges—$T_{1\rho}$ quantification in cartilage can provide valuable information related with biochemical changes in cartilage matrix. In particular, compared to more established T_2 relaxation time, $T_{1\rho}$ provides a larger dynamic range and a more sensitive detection of PG loss at early stages of cartilage degeneration. Similar as T_2 quantification, $T_{1\rho}$ quantification requires no contrast agent injection and no special hardware, therefore has great potential to be used in clinical applications or trials. Technical challenges of $T_{1\rho}$ quantification include high energy deposited to tissue (high SAR), especially at high and ultra high field strength.

Magnetization transfer (MT) and chemical exchange-dependent saturation transfer (CEST) MRI

MR imaging techniques based on magnetization transfer (MT) are sensitive to marcomolecular changes in tissues by exploring the exchange of magnetization between the pool of semisolid macromolecule associated protons and the pool of more free or liquid protons associated with bulk water (66). During MT experiments, the macromolecule-bounded protons are preferentially saturated with selective off-resonance RF pulses. The exchange of magnetization that transfers macromolecular saturation to the liquid proton pool produces an observable decrease in the longitudinal magnetization of the liquid spins. The magnetization exchange can occur via dipolar coupling or via chemical exchange. The most common parameter to quantify the amount of MT is by calculating the MT ratio (MTR) of the signal intensity before and after saturation.

The magnetization transfer effect in cartilage has been attributed primarily to collagen (67), while studies showed that changes in PG concentration and tissue structure also contribute to changes in MT ratio in cartilage (68). It is worthy of noting that although MTR provides valuable information regarding tissue composition, MTR is not an intrinsic MR property of tissue. This parameter is reflective of a complex combination of the sequence, tissue relaxation and MT parameters. In an effort to decouple the contribution of each of these

parameters, quantitative magnetization transfer (qMT) techniques have been proposed (69, 70). These methods derive the fraction of exchanging protons that are bound to macromolecules and the exchange rate between the bound and free pool based on the two-compartment model. A recent study applied qMT techniques in bovine cartilage and revealed that in the top layer of cartilage, the bound pool fraction was moderately correlated with PG content while the cross-relaxation rate and the longitudinal relaxation time were moderately correlated with collagen (71). More studies in the future are warranted to examine the feasibility and validity of qMT in assessing matrix composition of healthy and degenerated cartilage.

Chemical exchange dependent saturation transfer (CEST) imaging is a relatively new magnetic resonance imaging contrast approach (72). In CEST experiments, exogenous or endogenous compounds containing either exchangeable protons or exchangeable molecules are selectively saturated and after transfer of this saturation upon chemical exchange to the bulk water, detected indirectly through the water signal with enhanced sensitivity. In CEST MRI, transfer of magnetization is studied in mobile compounds instead of semisolids in contrast to conventional MT.

In order to account for direct saturation of water and background magnetization transfer that is related to mechanism other than chemical exchange, such as nuclear overhauser effect (NOE) in cartilage (73), two images are normally acquired in CEST experiments. One with a saturation pulse applied at the resonance frequency of interest ($-\delta$), and the other acquired with an equal frequency offset but applied on the other side of the bulk water peak (δ). The CEST effect was then quantified as the difference of these two images (73).

In cartilage, CEST exploits the exchangeable protons, including NH, OH and NH_2 proton groups, on the GAG side chains of PG (73, 74), and was termed as gagCEST. Ling et al. showed that –OH at $\delta = -1.0$ ppm, where δ is the frequency offset relative to the water, among other labile protons, can be used to monitor GAG concentration in cartilage *in vivo* (73). gagCEST revealed difference in GAG concentration between trypsin PG-depleted cartilage vs controls, and low GAG concentration *in vivo* with focal cartilage lesion (73), Fig. 10. At 7T, a strong correlation ($r = 0.701$) was found between ratios of signal intensity from native cartilage to signal intensity from repair tissue obtained with gagCEST (asymmetries in gagCEST z-spectra summed over all offsets from 0 to 1.3 ppm) or ^{23}Na imaging (74), which suggested the specificity of gagCEST for detecting GAG concentration.

gagCEST is a promising new method of evaluating cartilage matrix composition, with high specificity to GAG concentration and no need of contrast agent injection. However, the sensitivity to multiple factors, including pH changes, changes in hydration and collagen that may also change the exchange rate of –OH protons, and to pulse sequence parameters complicates the interpretation of gagCEST and comparison studies between laboratories. In addition, the field inhomogeneity, susceptibility-induced artifacts and motion may confound the results from gagCEST experiments. Further, at 3T, the slow-to-intermediate exchange condition, $\Delta\omega > k$ (where $\Delta\omega$ is the chemical shift of the solute spin relative to bulk water proton, and k is the exchange rate of solute spin), which is needed to be efficiently observe CEST effect, is not fulfilled for –OH protons with exchange site at 1ppm. The CEST effect is expected to increase at ultra high field strength such as 7T. The advantage includes the larger frequency separation for better adherence to the slow-exchange condition and reduced interference of direct water saturation, and the limitation includes the increase in power deposition.

Diffusion Imaging

Diffusion MRI measures Brownian motion of water molecules in tissues, which provides a non-invasive method for evaluating microscopic cellular structures of the tissue. Diffusion-weighted images provide a new contrast qualitatively related to tissue properties. Diffusion tensor imaging (DTI) where diffusion weighted images are acquired in multiple directions can provide quantitative information, including the mean diffusivity (MD) or apparent diffusion coefficient (ADC), indicating the degree of water diffusion, and the fractional anisotropy (FA), indicating the anisotropy of water diffusion in different orientations.

Ex vivo studies have documented promising results that MRI diffusion parameters may be sensitive to both the PG content and the collagen architecture within cartilage matrix, and therefore can be promising indicators of early degeneration of the tissue (75–77). Zonal variation was observed where ADC continuously decreased and FA increased from the articular surface to the bone-cartilage interface (77). The collagen fiber architecture has been shown to be the primary source of the anisotropy of diffusion (75, 76). The primary eigenvector of the diffusion tensor (ie, the eigenvector associated with the largest eigenvalue) has been shown to correlate with the orientation of the collagen fibrils using polarized light microscopy (PLM) (76) and scanning electron microscopy (77). Loss of PG caused significant increases of mean diffusivity and minimal changes in FA, while collagen depletion led to changes of ADC, fractional anisotropy (FA), and primary eigenvector (75).

Despite promising results from *ex vivo* studies, *in vivo* quantification of diffusion coefficients in cartilage are rather limited due to the short T_2 and consequently low SNR in cartilage, as well as spatial distortions arising from the sensitivity of the EPI trajectory to B_0 field inhomogeneity (therefore the commonly used EPI based diffusion sequences are not optimal for cartilage imaging). Very recently, Staroswiecki et al. proposed a method for *in vivo* simultaneous quantification of cartilage T_2 and apparent diffusion coefficients by modifying the spoiler gradient area and flip angle of the double echo steady state (DESS) sequence (78). Data acquired in phantoms and *in vivo* healthy knees at 3T showed good agreement with quantification using standard spin-echo sequences (78). Raya et al. performed *in vivo* DTI of cartilage at 7T using line-scan techniques (79). The test-retest reproducibility was 8.1% for mean ADC and 9.7% for FA. Mean ADC and FA differed significantly ($P < .01$) between the OA and healthy populations, while T_2 did not in their study cohort (79), Fig. 11. These studies demonstrated the feasibility of performing *in vivo* diffusion imaging in cartilage.

Diffusion MRI, in particular DTI, has the advantage that multi-components of the cartilage matrix including PG concentration and collagen network orientation and fraction can be quantified from one sequence. The major challenges for *in vivo* diffusion MRI of cartilage include the low SNR due to the short T_2 relaxation time of the tissue, requirement of high resolution due to small dimension of cartilage and the sensitivity of diffusion MRI to motion, and long acquisition time. Further studies are warranted to evaluate the reliability and reproducibility of *in vivo* diffusion parameter quantification and to evaluate its capability in diagnosing and monitoring cartilage degeneration.

Sodium Imaging

In addition to the proton MRI methods, sodium (^{23}Na) MRI has also been developed to evaluate cartilage matrix composition, in particular PG concentration, which was reviewed in detail by Borthakur et al. (80). As discussed earlier, the GAG side chains of the PG are negatively charged, which concentrates cations including Na+ and K+ in the cartilaginous interstitial fluid. Based on the ideal Donnan theory, the fixed charge density (FCD), which is

correlated with GAG concentration, can be estimated based on sodium content (81, 82). Therefore, sodium can serve as an attractive natural endogenous contrast for PG evaluation.

Compared to proton MRI, sodium MRI, however, suffers from inherent low SNR due to 1) low concentrations *in vivo* (<300 mM of ^{23}Na vs. 50 M of ^{1}H in healthy cartilage); 2) a four times lower gyromagnetic ratio (11.262 MHz/T of ^{23}Na vs 42.575 MHz/T for ^{1}H); and 3) the ultra-short T_2 and T_2* relaxation times (short T_2 and T_2* component less than 2 ms, and long T_2 and T_2* component less than 15ms). Thus, it is highly challenging to acquire *in vivo* sodium MR images with adequate SNR and spatial resolution under a clinically reasonable scan time. Higher static magnetic field strengths, dedicated coils and optimal pulse sequences are essential for *in vivo* sodium MRI.

Three dimensional gradient echo sequences have demonstrated the feasibility of sodium MRI of the human knee *in vivo* (80). However, these approaches are suboptimal as they required long TE values of 2–6.4 ms. Three dimensional projection imaging permits extremely short TE and has been implemented for sodium knee imaging either with twisted projection imaging (TPI, TE = 0.4 ms) (80), straight radial projections (TE = 0.16 ms) (83), or 3D cones (TE = 0.6 ms) (84). Nonselective hard RF pulses are also essential to achieve short TE in these 3D projection sequences. Using these techniques, normally at 3T and/or 7T, images can be acquired approximately within 15–30 minutes with a reasonable SNR and spatial resolution, Fig. 12 (SNR <30 with nominal resolution 3.4 mm^3, scan time <14 minutes using a quadrature 23Na coil at 7T (83); SNR~7 at 3T using a sodium-only coil and SNR~17 at 7T using a dual-tuned sodium/proton surface coil. Both 3T and 3 T measures had TE = 0.6 ms, nominal resolution 2 mm^3, scan time <26 minutes (84)).

In addition to the above efforts to reduce the TE to the lowest limit allowed by hardware, a recent study suggested an optimization of sodium SNR under SAR constraints with a shorter “steady-state” TR and smaller flip angles to take advantage of short sodium T_1 (~ 24 ms at 4T) (85). This shorter TR allowed more data averaging (although it meanwhile increased the TE due to SAR limit), which resulted in an approximately 30% SNR increase compared to “fully relaxed” parameters. At 4.7 T, using this projection acquisition in the steady state (PASS) sequence, sodium images (TR/TE = 30/0.185 ms), with SNR 8–10 were acquired within 9 minutes (85).

Sodium content in cartilage measured by NMR and MRI was highly correlated with measures from inductively coupled plasma emission spectroscopy (ICP) (81) and standard dimethylmethylene blue PG assays (82), respectively. Using relaxation normalized calibration phantoms, sodium absolute concentration and then FCD were quantified. In trypsin digested bovine cartilage, with over a 20% PG depletion, sodium image signal change correlated significantly with the observed PG loss (80). Improved methods were suggested later to correct for B_1 inhomogeneity, as well as for $T_1$and T_2* weighting during sodium quantification, and showed the feasibility of using sodium MRI to distinguish early degenerated cartilage using *in vivo* data from controls *in vivo* at 4.7 T with a surface coil (80). At 7 T, sodium concentrations were reduced significantly in OA subjects (n = 3) compared to controls (n = 5) by approximately 30%–60%, depending on the degree of cartilage degeneration (83).

The major advantage of sodium MR imaging of cartilage is its high specificity to PG content without the need for any exogenous contrast. Moreover, the low sodium content (<50 mmol/L) of surrounding structures in the joint enables visualization of the cartilage with very high tissue contrast. However, sodium MRI is primarily limited by special hardware requirements and by inherently low sensitivity at the standard clinical field strength of 1.5T. With the

increasing availability of scanners with high field strength (3 T or higher) it may find more general applications.

Ultra Short Echo Imaging Methods

Sequences that acquire data with ultra-short or negligible time between excitation and data acquisition are designed to image tissue components with very short T_2 of a few milliseconds or less (86), which are otherwise 'invisible' with conventional MR sequences. In addition to cortical bone and tendons, the ultra-short echo (UTE) methods have been applied to cartilage, menisci and vertebral disc, as reviewed by Bae et al. (87). In cartilage, with the exception of the laminar splendens, the T_2 relaxation times decrease from the superficial zone to the deep zone as discussed previously. In the calcified zone close to the bone-cartilage interface, the T_2 relaxation times can be 10 ms or less. Changes within these regions may be important in early detection of cartilage degeneration.

The typical ultra-short echo (UTE) sequences apply half excitation pulses and data are acquired on the gradient ramp to keep a minimal TE, normally from a few micro- seconds (μs) to less than 100 μs. The data acquisition was developed with both 2D and 3D implementation, including 2D radial, twisted radial or spiral acquisition, and 3D projection reconstruction (3D PR), twisted projection imaging (TPI) and hybrid methods such as acquisition-weighted stack of spirals (87). Multiple techniques for long-T_2 component suppression in UTE were proposed in order to improve the contrast and visualization of short T_2 component, including dual echo acquisition with echo or scaled echo subtraction, methods based on RF pulses that selectively saturate or null long T_2-component for saturation and their modifications (86, 88).

More recently, UTE sequences have been employed for quantifying T_2* by Williams et al. (89) and $T_{1\rho}$ by Du et al. (90) in cartilage and other MSK tissues with short T_2 such as Achilles tendon and meniscus. The root-mean-square average coefficients of variation (RMSA-CV) of *in vivo* UTE-T_2* measures in cartilage was reported to be 8%, 6%, 16% for full-thickness, superficial and deep cMFC ROIs, corresponding to absolute errors (SD) of 1.2, 1.5, 1.5 ms, respectively (89). These sequences also have potential to quantify the relaxation times and the fractions of short and long water components in cartilage and other tissues.

REPAIR AND REGENERATION

MR methods especially those characterizing changes in the extra-cellular matrix play an important role in assessing cartilage repair (91). Microfracture is a frequently used technique for the repair of articular cartilage lesions of the knee, which is performed by inducing multiple penetrating injuries into the subchondral bone. Pluripotent mesenchymal progenitor cells migrate into the injury area, which subsequently form reparative fibrocartilage. Such generated fibrocartilage typically lacks stratification of hyaline cartilage matrix structure. In contrast, other techniques, including mosaicplasty, autologous chondrocyte transplantation (ACT) or matrix-associated autologous chondrocyte transplantation (MACT) are expected to generate more hyaline cartilage with stratification of matrix structure.

Marlovits et al. developed a Magnetic Resonance Observation of Cartilage Repair Tissue (MOCART) classification system that defined nine variables to describe the morphology and signal intensity of the repair tissue compared to the adjacent native cartilage. Excellent interobserver reproducibility of MOCART grading was reported and the gradings were correlated to clinical outcomes evaluated by visual analog score (VAS) and the knee injury and osteoarthritis outcome score (KOOS) in a 2-year longitudinal study (92).

In a prospective 2-year study in symptomatic patients with isolated full-thickness articular cartilage defects treated with the microfracture technique outcomes, clinical rating and MRI was combined. MRI showed good repair-tissue fill in the defect in thirteen patients (54%), moderate fill in seven (29%), and poor fill in four patients (17%) and correlated with the knee function scores (93). A multi-modal approach using T_2, diffusion weighted imaging and grading of MR images has been used for assessing post- operative cartilage. While grading did not show differences between the two repair techniques, microfracture therapy and MACT, T_2-mapping showed lower T_2 values after microfracture, and diffusion weighted imaging between healthy cartilage and cartilage repair tissue in both procedures (94). Mamisch et al. (95) prospectively used T_2 cartilage maps to study the effect of unloading during the MR scan in the postoperative follow-up of patients after MACT of the knee joint. They demonstrated that T_2 values change with the time of unloading during the MR scan, and this difference was more pronounced in repair tissue. The difference between the repair and control tissue was also greater after longer unloading times, implying that assessment of cartilage repair is affected by the timing of the image acquisition relative to unloading the joint. A combined $T_{1\rho}$ and T_2 study examining repaired and the surrounding cartilage has demonstrated differences in cartilage after microfracture and mosaicplasty 3–6 months and after a year (96), Fig. 13.

Articular cartilage has very limited intrinsic regenerative capacity, making cell-based therapy a possible approach for cartilage repair. Tissue engineered collagen matrix seeded with autogenous chondrocytes designed for the repair of hyaline articular cartilage have also been proposed and early studies combining MR grading and quantitative T_2 mapping have been used to assess the impact of such repair (97). In addition to fill efficacy the layered appearance or partial stratification of T_2 as a result of collagen orientation was detected in this study for 2 patients at 12 months and 4 patients at 24 months. Cell tracking can be a major step towards unraveling and improving the repair process of some of these therapies. Micrometer sized (MPIOs) and superparamagnetic iron oxides (SPIO) for labeling bone marrow-derived mesenchymal stem cells regarding effectivity, cell viability, long-term metabolic cell activity, chondrogenic differentiation has been studied (98, 99). MPIO labeling results in efficient contrast uptake and signal loss that can be visualized and quantitatively characterized via MRI. SPGR imaging of implanted cells results in *ex vivo* detection within native tissue, and $T_{1\rho}$ imaging is unaffected by the presence of labeled cells immediately following implantation. MPIO labeling does not affect quantitative GAG production during chondrogenesis, but iron aggregation hinders extracellular matrix visualization (98). Similarly, SPIO labeling was effective and did not impair any of the studied safety aspects, and injected and implanted SPIO-labeled cells can be accurately be visualized by MRI in a clinically relevant sized joint (100).

CONCLUSIONS

Quantitative MRI can provide non-invasive measurement of cartilage morphology as well as early changes within the matrix, which should be used concurrently for evaluating cartilage degeneration during OA. In particular, measures that detect early changes in the matrix may provide novel imaging markers for cartilage degeneration at early and potentially reversible stages. The most value of these advanced measures probably lies in evaluating subjects who are at early stages of the disease, and have a high risk of fast progression, such as those with obesity or with acute injuries. Such imaging markers will provide critical evaluation and monitoring for early intervention and prevention of the disease of OA. The quantitative MRI can be also effective in augmenting the longitudinal assessment of cohorts at risk for premature osteoarthritis, such as developmental dysplasia of the hip, femoroacetabular impingement, and patellofemoral dysmorphism.

While univariate analysis of each MR parameters discussed in this paper demonstrated promising results, combing them using advanced statistical analysis method will provide multparametric evaluation and integrate information related with different aspects of the cartilage matrix, which has the potential to further improve our capability to distinguish degenerated cartilage from controls, as well as to monitor subtle changes after interventions.

Current advanced MRI methods for quantifying matrix changes normally require a long acquisition time and have a limited spatial resolution. Further technique development to increase the spatial resolution, the signal-to-noise ratio, and to reduce the acquisition time will facilitate translating these techniques into clinical applications.

Another critical issue for applying these advanced MRI techniques in clinical trial or studies is the standardization of the acquisition and post-processing techniques. As discussed earlier, quantification variation can be caused by different scanner models, different sequence types and different post-processing methodologies. The efforts of having standardized imaging and image processing protocols need to be synthesized between academic and industrial communities. More longitudinal and multicenter large-scale studies are warranted to evaluate the reliability (repeatability), validity, sensitivity and specificity of advanced MRI measures as biomarkers for evaluating cartilage degeneration in OA.

Acknowledgments

Supported in part by National Institutes of Health grants K25 AR053633, R01 AR46905, R01 AG17762, U01 AR055079, R21 AR056773, P50 AR060752, the Aircast Foundation, Pfizer Inc, GlaxoSmithKline Inc and GE Healthcare.

References

1. Dijkgraaf LC, de Bont LG, Boering G, Liem RS. The structure, biochemistry, and metabolism of osteoarthritic cartilage: a review of the literature. J Oral Maxillofac Surg. 1995; 53(10):1182–1192. [PubMed: 7562173]
2. Goldring M, Goldring S. Osteoarthritis. J Cell Physiol. 2007; 213(3):626–634. [PubMed: 17786965]
3. Peterfy CG, Guermazi A, Zaim S, Tirman PF, Miaux Y, White D, et al. Whole-Organ Magnetic Resonance Imaging Score (WORMS) of the knee in osteoarthritis. Osteoarthritis Cartilage. 2004; 12(3):177–190. [PubMed: 14972335]
4. Hunter DJ, Lo GH, Gale D, Grainger AJ, Guermazi A, Conaghan PG. The reliability of a new scoring system for knee osteoarthritis MRI and the validity of bone marrow lesion assessment: BLOKS (Boston Leeds Osteoarthritis Knee Score). Ann Rheum Dis. 2008; 67(2):206–211. Epub 2007/05/03. ard.2006.066183 [pii]. 10.1136/ard.2006.066183 [PubMed: 17472995]
5. Eckstein F, Adam C, Sittek H, Becker C, Milz S, Schulte E, et al. Non-invasive determination of cartilage thickness throughout joint surfaces using magnetic resonance imaging. J Biomech. 1997; 30(3):285–289. Epub 1997/03/01. [PubMed: 9119830]
6. Stammberger T, Eckstein F, Michaelis M, Englmeier KH, Reiser M. Interobserver reproducibility of quantitative cartilage measurements: comparison of B-spline snakes and manual segmentation. Magn Reson Imaging. 1999; 17(7):1033–1042. [PubMed: 10463654]
7. Lynch, JA.; Zaim, S.; Zhao, J.; Stork, A.; Peterfy, CG.; Genant, HK., editors. SPIE, Medical Imaging. San Diego, CA: 2000. Cartilage segmentation of 3D MRI scans of the osteoarthritic knee combining user knowledge and active contours.
8. Grau V, Mewes AU, Alcaniz M, Kikinis R, Warfield SK. Improved watershed transform for medical image segmentation using prior information. IEEE Trans Med Imaging. 2004; 23(4):447–458. [PubMed: 15084070]
9. Pakin, SK.; Tamez-Pena, JG.; Totterman, S.; Parker, KJ., editors. SPIE, Medical Imaging. San Diego, CA: 2002. Segmentation, surface extraction, and thickness computation of articular cartilage.

10. Warfield SK, Kaus M, Jolesz FA, Kikinis R. Adaptive, template moderated, spatially varying statistical classification. Med Image Anal. 2000; 4(1):43–55. [PubMed: 10972320]
11. Carballido-Gamio J, Bauer JS, Stahl R, Lee KY, Krause S, Link TM, et al. Inter-subject comparison of MRI knee cartilage thickness. Med Image Anal. 2008; 12(2):120–135. [PubMed: 17923429]
12. Ateshian GA, Soslowsky LJ, Mow VC. Quantitation of articular surface topography and cartilage thickness in knee joints using stereophotogrammetry. J Biomech. 1991; 24(8):761–776. Epub 1991/01/01. [PubMed: 1918099]
13. Pelletier JP, Raynauld JP, Berthiaume MJ, Abram F, Choquette D, Haraoui B, et al. Risk factors associated with the loss of cartilage volume on weight-bearing areas in knee osteoarthritis patients assessed by quantitative magnetic resonance imaging: a longitudinal study. Arthritis Res Ther. 2007; 9(4):R74. Epub 2007/08/04. ar2272 [pii]. 10.1186/ar2272 [PubMed: 17672891]
14. Carballido-Gamio J, Link T, Majumdar S. New techniques for cartilage magnetic resonance imaging relaxation time analysis: texture analysis of flattened cartilage and localized intra- and inter-subject comparisons. Magn Reson Med. 2008; 59(6):1472–1477. [PubMed: 18506807]
15. Cohen ZA, Mow VC, Henry JH, Levine WN, Ateshian GA. Templates of the cartilage layers of the patellofemoral joint and their use in the assessment of osteoarthritic cartilage damage. Osteoarthritis Cartilage. 2003; 11(8):569–579. [PubMed: 12880579]
16. Eckstein F, Wirth W, Nevitt MC. Recent advances in osteoarthritis imaging-the Osteoarthritis Initiative. Nat Rev Rheumatol. 2012; 8(10):622–630. [PubMed: 22782003]
17. Mankin HJ, Thrasher AZ. Water content and binding in normal and osteoarthritic human cartilage. J Bone Joint Surg Am. 1975; 57(1):76–80. Epub 1975/01/01. [PubMed: 1123375]
18. Bashir A, Gray ML, Burstein D. Gd-DTPA2- as a measure of cartilage degradation. Magn Reson Med. 1996; 36(5):665–673. [PubMed: 8916016]
19. Gray ML, Burstein D, Kim YJ, Maroudas A. 2007 Elizabeth Winston Lanier Award Winner. Magnetic resonance imaging of cartilage glycosaminoglycan: basic principles, imaging technique, and clinical applications. J Orthop Res. 2008; 26(3):281–291. Epub 2007/09/19. 10.1002/jor.20482 [PubMed: 17876836]
20. Siversson C, Tiderius CJ, Neuman P, Dahlberg L, Svensson J. Repeatability of T1-quantification in dGEMRIC for three different acquisition techniques: two-dimensional inversion recovery, three-dimensional look locker, and three-dimensional variable flip angle. J Magn Reson Imaging. 2010; 31(5):1203–1209. Epub 2010/05/01. 10.1002/jmri.22159 [PubMed: 20432357]
21. Burstein D, Velyvis J, Scott KT, Stock KW, Kim YJ, Jaramillo D, et al. Protocol issues for delayed Gd(DTPA)(2-)-enhanced MRI (dGEMRIC) for clinical evaluation of articular cartilage. Magn Reson Med. 2001; 45(1):36–41. Epub 2001/01/09. [pii]. 10.1002/1522-2594(200101)45:1<36::AID-MRM1006>3.0.CO;2-W [PubMed: 11146483]
22. Williams A, Sharma L, McKenzie CA, Prasad PV, Burstein D. Delayed gadolinium-enhanced magnetic resonance imaging of cartilage in knee osteoarthritis: findings at different radiographic stages of disease and relationship to malalignment. Arthritis Rheum. 2005; 52(11):3528–3535. Epub 2005/10/29. 10.1002/art.21388 [PubMed: 16255024]
23. Anandacoomarasamy A, Giuffre BM, Leibman S, Caterson ID, Smith GS, Fransen M, et al. Delayed gadolinium-enhanced magnetic resonance imaging of cartilage: clinical associations in obese adults. J Rheumatol. 2009; 36(5):1056–1062. Epub 2009/04/17. jrheum.080997 [pii]. 10.3899/jrheum.080997 [PubMed: 19369468]
24. Ericsson YB, Tjornstrand J, Tiderius CJ, Dahlberg LE. Relationship between cartilage glycosaminoglycan content (assessed with dGEMRIC) and OA risk factors in meniscectomized patients. Osteoarthritis Cartilage. 2009; 17(5):565–570. Epub 2008/12/09. S1063-4584(08)00335-X [pii]. 10.1016/j.joca.2008.10.009 [PubMed: 19058980]
25. Tiderius CJ, Olsson LE, Nyquist F, Dahlberg L. Cartilage glycosaminoglycan loss in the acute phase after an anterior cruciate ligament injury: delayed gadolinium-enhanced magnetic resonance imaging of cartilage and synovial fluid analysis. Arthritis Rheum. 2005; 52(1):120–127. [PubMed: 15641092]
26. Fleming BC, Oksendahl HL, Mehan WA, Portnoy R, Fadale PD, Hulstyn MJ, et al. Delayed Gadolinium-Enhanced MR Imaging of Cartilage (dGEMRIC) following ACL injury.

Osteoarthritis Cartilage. 2010; 18(5):662–667. Epub 2010/03/02. S1063-4584(10)00038-5 [pii]. 10.1016/j.joca.2010.01.009 [PubMed: 20188685]

27. Mamisch TC, Kain MS, Bittersohl B, Apprich S, Werlen S, Beck M, et al. Delayed gadolinium-enhanced magnetic resonance imaging of cartilage (dGEMRIC) in Femoacetabular impingement. J Orthop Res. 2011; 29(9):1305–1311. Epub 2011/03/26. 10.1002/jor.21371 [PubMed: 21437964]
28. Jessel RH, Zilkens C, Tiderius C, Dudda M, Mamisch TC, Kim YJ. Assessment of osteoarthritis in hips with femoroacetabular impingement using delayed gadolinium enhanced MRI of cartilage. J Magn Reson Imaging. 2009; 30(5):1110–1115. Epub 2009/10/27. 10.1002/jmri.21830 [PubMed: 19856439]
29. Kim YJ, Jaramillo D, Millis MB, Gray ML, Burstein D. Assessment of early osteoarthritis in hip dysplasia with delayed gadolinium-enhanced magnetic resonance imaging of cartilage. J Bone Joint Surg Am. 2003; 85-A(10):1987–92. Epub 2003/10/18. [PubMed: 14563809]
30. Pai A, Li X, Majumdar S. A comparative study at 3 T of sequence dependence of T2 quantitation in the knee. Magn Reson Imaging. 2008; 26(9):1215–1220. [PubMed: 18502073]
31. Regatte RR, Akella SV, Borthakur A, Kneeland JB, Reddy R. Proteoglycan depletion-induced changes in transverse relaxation maps of cartilage: comparison of T2 and T1rho. Acad Radiol. 2002; 9(12):1388–1394. [PubMed: 12553350]
32. Xia Y. Relaxation anisotropy in cartilage by NMR microscopy (muMRI) at 14- microm resolution. Magn Reson Med. 1998; 39(6):941–949. [PubMed: 9621918]
33. Nieminen MT, Rieppo J, Toyras J, Hakumaki JM, Silvennoinen J, Hyttinen MM, et al. T2 relaxation reveals spatial collagen architecture in articular cartilage: a comparative quantitative MRI and polarized light microscopic study. Magn Reson Med. 2001; 46(3):487–493. Epub 2001/09/11. [pii]. 10.1002/mrm.1218 [PubMed: 11550240]
34. Reiter DA, Roque RA, Lin PC, Doty SB, Pleshko N, Spencer RG. Improved specificity of cartilage matrix evaluation using multiexponential transverse relaxation analysis applied to pathomimetically degraded cartilage. NMR Biomed. 2011; 24(10):1286–1294. Epub 2011/04/06. 10.1002/nbm.1690 [PubMed: 21465593]
35. Wang N, Xia Y. Dependencies of multi-component T2 and T1rho relaxation on the anisotropy of collagen fibrils in bovine nasal cartilage. J Magn Reson. 2011; 212(1):124–132. Epub 2011/07/27. S1090-7807(11)00218-7 [pii]. 10.1016/j.jmr.2011.06.031 [PubMed: 21788148]
36. Dardzinski BJ, Mosher TJ, Li S, Van Slyke MA, Smith MB. Spatial variation of T2 in human articular cartilage. Radiology. 1997; 205(2):546–550. [PubMed: 9356643]
37. Li X, Pai A, Blumenkrantz G, Carballido-Gamio J, Link T, Ma B, et al. Spatial distribution and relationship of T1rho and T2 relaxation times in knee cartilage with osteoarthritis. Magn Reson Med. 2009; 61(6):1310–1318. Epub 2009/03/26. 10.1002/mrm.21877 [PubMed: 19319904]
38. Mosher T, Liu Y, Yang Q, Yao J, Smith R, Dardzinski B, et al. Age dependency of cartilage magnetic resonance imaging T2 relaxation times in asymptomatic women. Arthritis Rheum. 2004; 50(9):2820–2828. [PubMed: 15457450]
39. Mosher TJ, Collins CM, Smith HE, Moser LE, Sivarajah RT, Dardzinski BJ, et al. Effect of gender on in vivo cartilage magnetic resonance imaging T2 mapping. J Magn Reson Imaging. 2004; 19(3):323–328. Epub 2004/03/03. 10.1002/jmri.20013 [PubMed: 14994301]
40. Li X, Ma C, Link T, Castillo D, Blumenkrantz G, Lozano J, et al. In vivo T1rho and T2 mapping of articular cartilage in osteoarthritis of the knee using 3 Tesla MRI. Osteoarthritis and Cartilage. 2007; 15(7):789–797. [PubMed: 17307365]
41. Koff MF, Amrami KK, Kaufman KR. Clinical evaluation of T2 values of patellar cartilage in patients with osteoarthritis. Osteoarthritis Cartilage. 2007; 15(2):198–204. Epub 2006/09/05. S1063-4584(06)00232-9 [pii]. 10.1016/j.joca.2006.07.007 [PubMed: 16949313]
42. Bolbos R, Zuo J, Banerjee S, Link T, Ma C, Li X, et al. Relationship between trabecular bone structure and articular cartilage morphology and relaxation times in early OA of the knee joint using parallel MRI at 3 T. Osteoarthritis Cartilage. 2008; 16(10):1150–1159. [PubMed: 18387828]
43. Lammentausta E, Kiviranta P, Toyras J, Hyttinen MM, Kiviranta I, Nieminen MT, et al. Quantitative MRI of parallel changes of articular cartilage and underlying trabecular bone in degeneration. Osteoarthritis Cartilage. 2007; 15(10):1149–1157. Epub 2007/05/16. S1063-4584(07)00123-9 [pii]. 10.1016/j.joca.2007.03.019 [PubMed: 17502160]

44. Mosher TJ, Liu Y, Torok CM. Functional cartilage MRI T2 mapping: evaluating the effect of age and training on knee cartilage response to running. Osteoarthritis Cartilage. 2010; 18(3):358–364. Epub 2009/12/02. S1063-4584(09)00306-9 [pii]. 10.1016/j.joca.2009.11.011 [PubMed: 19948266]
45. Subburaj K, Kumar D, Souza RB, Alizai H, Li X, Link TM, et al. The Acute Effect of Running on Knee Articular Cartilage and Meniscus Magnetic Resonance Relaxation Times in Young Healthy Adults. Am J Sports Med. 2012; 9(40):2134–2141. Epub 2012/06/26. 0363546512449816 [pii]. 10.1177/0363546512449816 [PubMed: 22729505]
46. Potter HG, Jain SK, Ma Y, Black BR, Fung S, Lyman S. Cartilage injury after acute, isolated anterior cruciate ligament tear: immediate and longitudinal effect with clinical/MRI follow-up. Am J Sports Med. 2012; 40(2):276–285. Epub 2011/09/29. 10.1177/0363546511423380 [PubMed: 21952715]
47. Schneider E, NessAiver M, White D, Purdy D, Martin L, Fanella L, et al. The osteoarthritis initiative (OAI) magnetic resonance imaging quality assurance methods and results. Osteoarthritis Cartilage. 2008; 16(9):994–1004. Epub 2008/04/22. S1063-4584(08)00050-2 [pii]. 10.1016/j.joca.2008.02.010 [PubMed: 18424108]
48. Hovis KK, Stehling C, Souza RB, Haughom BD, Baum T, Nevitt M, et al. Physical activity is associated with magnetic resonance imaging-based knee cartilage T2 measurements in asymptomatic subjects with and those without osteoarthritis risk factors. Arthritis Rheum. 2011; 63(8):2248–2256. Epub 2011/05/04. 10.1002/art.30419 [PubMed: 21538328]
49. Pan J, Pialat JB, Joseph T, Kuo D, Joseph GB, Nevitt MC, et al. Knee Cartilage T2 Characteristics and Evolution in Relation to Morphologic Abnormalities Detected at 3-T MR Imaging: A Longitudinal Study of the Normal Control Cohort from the Osteoarthritis Initiative. Radiology. 2011; 261(2):507–515. Epub 2011/09/09. radiol.11102234 [pii]. 10.1148/radiol.11102234 [PubMed: 21900614]
50. Joseph GB, Baum T, Alizai H, Carballido-Gamio J, Nardo L, Virayavanich W, et al. Baseline mean and heterogeneity of MR cartilage T(2) are associated with morphologic degeneration of cartilage, meniscus, and bone marrow over 3years - data from the Osteoarthritis Initiative. Osteoarthritis Cartilage. 2012; 20(7):727–735. Epub 2012/04/17. S1063-4584(12)00780-7 [pii]. 10.1016/j.joca.2012.04.003 [PubMed: 22503812]
51. Li X, Han E, Busse R, Majumdar S. In vivo T1rho mapping in cartilage using 3D magnetization-prepared angle-modulated partitioned k-space spoiled gradient echo snapshots (3D MAPSS). Magn Reson Med. 2008; 59(2):298–307. [PubMed: 18228578]
52. Witschey W, Borthakur A, Elliott M, Fenty M, Sochor M, Wang C, et al. T1rho-prepared balanced gradient echo for rapid 3D T1rho MRI. J Magn Reson Imaging. 2008; 28(3):744–754. [PubMed: 18777535]
53. Regatte RR, Akella SV, Wheaton AJ, Lech G, Borthakur A, Kneeland JB, et al. 3D-T1rho-relaxation mapping of articular cartilage: in vivo assessment of early degenerative changes in symptomatic osteoarthritic subjects. Acad Radiol. 2004; 11(7):741–749. [PubMed: 15217591]
54. Charagundla SR, Borthakur A, Leigh JS, Reddy R. Artifacts in T(1rho)-weighted imaging: correction with a self-compensating spin-locking pulse. J Magn Reson. 2003; 162(1):113–121. [PubMed: 12762988]
55. Chen W, Takahashi A, Han E. Quantitative T(1)(rho) imaging using phase cycling for B0 and B1 field inhomogeneity compensation. Magn Reson Imaging. 2011; 29(5):608–619. Epub 2011/04/29. S0730-725X(11)00064-6 [pii]. 10.1016/j.mri.2011.02.002 [PubMed: 21524869]
56. Li X, Cheng J, Lin K, Saadat E, Bolbos RI, Jobke B, et al. Quantitative MRI using T1rho and T2 in human osteoarthritic cartilage specimens: correlation with biochemical measurements and histology. Magn Reson Imaging. 2011; 29(3):324–334. Epub 2010/12/07. S0730-725X(10)00308-5 [pii]. 10.1016/j.mri.2010.09.004 [PubMed: 21130590]
57. Akella SV, Regatte RR, Wheaton AJ, Borthakur A, Reddy R. Reduction of residual dipolar interaction in cartilage by spin-lock technique. Magn Reson Med. 2004; 52(5):1103–1109. [PubMed: 15508163]
58. Duvvuri U, Goldberg AD, Kranz JK, Hoang L, Reddy R, Wehrli FW, et al. Water magnetic relaxation dispersion in biological systems: the contribution of proton exchange and implications for the noninvasive detection of cartilage degradation. Proc Natl Acad Sci U S A. 2001; 98(22): 12479–12484. [PubMed: 11606754]

59. Mlynarik V, Szomolanyi P, Toffanin R, Vittur F, Trattnig S. Transverse relaxation mechanisms in articular cartilage. J Magn Reson. 2004; 169(2):300–307. [PubMed: 15261626]
60. Kettunen M, Gröhn O, Silvennoinen M, Penttonen M, Kauppinen R. Effects of intracellular pH, blood, and tissue oxygen tension on T1rho relaxation in rat brain. Magn Reson Med. 2002; 48(3): 470–477. [PubMed: 12210911]
61. Mosher TJ, Zhang Z, Reddy R, Boudhar S, Milestone BN, Morrison WB, et al. Knee articular cartilage damage in osteoarthritis: analysis of MR image biomarker reproducibility in ACRIN-PA 4001 multicenter trial. Radiology. 2011; 258(3):832–842. Epub 2011/01/08. radiol.10101174 [pii]. 10.1148/radiol.10101174 [PubMed: 21212364]
62. Stahl R, Luke A, Li X, Carballido-Gamio J, Ma CB, Majumdar S, et al. T1rho, T2 and focal knee cartilage abnormalities in physically active and sedentary healthy subjects versus early OA patients--a 3.0-Tesla MRI study. Eur Radiol. 2009; 19(1):132–143. Epub 2008/08/19. 10.1007/s00330-008-1107-6 [PubMed: 18709373]
63. Zarins ZA, Bolbos RI, Pialat JB, Link TM, Li X, Souza RB, et al. Cartilage and meniscus assessment using T1rho and T2 measurements in healthy subjects and patients with osteoarthritis. Osteoarthritis Cartilage. 2010; 18(11):1408–1416. Epub 2010/08/11. S1063-4584(10)00249-9 [pii]. 10.1016/j.joca.2010.07.012 [PubMed: 20696262]
64. Li X, Ma C, Bolbos R, Stahl R, Lozano J, Zuo J, et al. Quantitative assessment of bone marrow edema pattern and overlying cartilage in knees with osteoarthritis and anterior cruciate ligament tear using MR imaging and spectroscopic imaging. J Magn Reson Imaging. 2008; 28(2):453–461. [PubMed: 18666183]
65. Li X, Kuo D, Theologis A, Carballido-Gamio J, Stehling C, Link TM, et al. Cartilage in anterior cruciate ligament-reconstructed knees: MR imaging T1{rho} and T2--initial experience with 1-year follow-up. Radiology. 2011; 258(2):505–514. Epub 2010/12/24. radiol.10101006 [pii]. 10.1148/radiol.10101006 [PubMed: 21177392]
66. Henkelman RM, Stanisz GJ, Graham SJ. Magnetization transfer in MRI: a review. NMR Biomed. 2001; 14(2):57–64. Epub 2001/04/26. [pii]. 10.1002/nbm.683 [PubMed: 11320533]
67. Kim DK, Ceckler TL, Hascall VC, Calabro A, Balaban RS. Analysis of water-macromolecule proton magnetization transfer in articular cartilage. Magn Reson Med. 1993; 29(2):211–215. [PubMed: 8429785]
68. Gray ML, Burstein D, Lesperance LM, Gehrke L. Magnetization transfer in cartilage and its constituent macromolecules. Magn Reson Med. 1995; 34(3):319–325. Epub 1995/09/01. [PubMed: 7500869]
69. Henkelman RM, Huang X, Xiang QS, Stanisz GJ, Swanson SD, Bronskill MJ. Quantitative interpretation of magnetization transfer. Magn Reson Med. 1993; 29(6):759–766. Epub 1993/06/01. [PubMed: 8350718]
70. Sled JG, Pike GB. Quantitative imaging of magnetization transfer exchange and relaxation properties in vivo using MRI. Magn Reson Med. 2001; 46(5):923–931. Epub 2001/10/25. [pii]. 10.1002/mrm.1278 [PubMed: 11675644]
71. Stikov N, Keenan KE, Pauly JM, Smith RL, Dougherty RF, Gold GE. Cross-relaxation imaging of human articular cartilage. Magn Reson Med. 2011; 66(3):725–734. Epub 2011/03/19. 10.1002/mrm.22865 [PubMed: 21416504]
72. van Zijl PC, Yadav NN. Chemical exchange saturation transfer (CEST): what is in a name and what isn't? Magn Reson Med. 2011; 65(4):927–948. Epub 2011/02/22. 10.1002/mrm.22761 [PubMed: 21337419]
73. Ling W, Regatte RR, Navon G, Jerschow A. Assessment of glycosaminoglycan concentration in vivo by chemical exchange-dependent saturation transfer (gagCEST). Proc Natl Acad Sci U S A. 2008; 105(7):2266–2270. Epub 2008/02/13. 0707666105 [pii]. 10.1073/pnas.0707666105 [PubMed: 18268341]
74. Schmitt B, Zbyn S, Stelzeneder D, Jellus V, Paul D, Lauer L, et al. Cartilage quality assessment by using glycosaminoglycan chemical exchange saturation transfer and (23)Na MR imaging at 7 T. Radiology. 2011; 260(1):257–264. Epub 2011/04/05. radiol.11101841 [pii]. 10.1148/radiol.11101841 [PubMed: 21460030]

75. Deng X, Farley M, Nieminen MT, Gray M, Burstein D. Diffusion tensor imaging of native and degenerated human articular cartilage. Magn Reson Imaging. 2007; 25(2):168–171. Epub 2007/02/06. S0730-725X(06)00321-3 [pii]. 10.1016/j.mri.2006.10.015 [PubMed: 17275610]
76. de Visser SK, Bowden JC, Wentrup-Byrne E, Rintoul L, Bostrom T, Pope JM, et al. Anisotropy of collagen fibre alignment in bovine cartilage: comparison of polarised light microscopy and spatially resolved diffusion-tensor measurements. Osteoarthritis Cartilage. 2008; 16(6):689–697. Epub 2007/11/21. S1063-4584(07)00315-9 [pii]. 10.1016/j.joca.2007.09.015 [PubMed: 18023211]
77. Raya JG, Arnoldi AP, Weber DL, Filidoro L, Dietrich O, Adam-Neumair S, et al. Ultra-high field diffusion tensor imaging of articular cartilage correlated with histology and scanning electron microscopy. MAGMA. 2011; 24(4):247–258. Epub 2011/06/02. 10.1007/s10334-011-0259-6 [PubMed: 21630094]
78. Staroswiecki E, Granlund KL, Alley MT, Gold GE, Hargreaves BA. Simultaneous estimation of T(2) and apparent diffusion coefficient in human articular cartilage in vivo with a modified three-dimensional double echo steady state (DESS) sequence at 3 T. Magn Reson Med. 2012; 67(4): 1086–1096. Epub 2011/12/20. 10.1002/mrm.23090 [PubMed: 22179942]
79. Raya JG, Horng A, Dietrich O, Krasnokutsky S, Beltran LS, Storey P, et al. Articular cartilage: in vivo diffusion-tensor imaging. Radiology. 2012; 262(2):550–559. Epub 2011/11/23. 10.1148/radiol.11110821 [PubMed: 22106350]
80. Borthakur A, Mellon E, Niyogi S, Witschey W, Kneeland J, Reddy R. Sodium and T1rho MRI for molecular and diagnostic imaging of articular cartilage. NMR Biomed. 2006; 19(7):781–821. [PubMed: 17075961]
81. Lesperance LM, Gray ML, Burstein D. Determination of fixed charge density in cartilage using nuclear magnetic resonance. J Orthop Res. 1992; 10(1):1–13. Epub 1992/01/01. 10.1002/jor.1100100102 [PubMed: 1309384]
82. Shapiro EM, Borthakur A, Gougoutas A, Reddy R. 23Na MRI accurately measures fixed charge density in articular cartilage. Magn Reson Med. 2002; 47(2):284–291. Epub 2002/01/26. [pii]. 10.1002/mrm.10054 [PubMed: 11810671]
83. Wang L, Wu Y, Chang G, Oesingmann N, Schweitzer ME, Jerschow A, et al. Rapid isotropic 3D-sodium MRI of the knee joint in vivo at 7T. J Magn Reson Imaging. 2009; 30(3):606–614. Epub 2009/08/28. 10.1002/jmri.21881 [PubMed: 19711406]
84. Staroswiecki E, Bangerter NK, Gurney PT, Grafendorfer T, Gold GE, Hargreaves BA. In vivo sodium imaging of human patellar cartilage with a 3D cones sequence at 3 T and 7 T. J Magn Reson Imaging. 2010; 32(2):446–451. Epub 2010/08/03. 10.1002/jmri.22191 [PubMed: 20677276]
85. Watts A, Stobbe RW, Beaulieu C. Signal-to-noise optimization for sodium MRI of the human knee at 4.7 Tesla using steady state. Magn Reson Med. 2011; 66(3):697–705. Epub 2011/03/26. 10.1002/mrm.22838 [PubMed: 21437972]
86. Gatehouse PD, Bydder GM. Magnetic resonance imaging of short T2 components in tissue. Clin Radiol. 2003; 58(1):1–19. Epub 2003/02/05. S0009926002004816 [pii]. [PubMed: 12565203]
87. Bae WC, Du J, Bydder GM, Chung CB. Conventional and Ultrashort Time-to-Echo Magnetic Resonance Imaging of Articular Cartilage, Meniscus, and Intervertebral Disk. Top Magn Reson Imaging. 2010; 21(5):275–289. Epub 2010/10/01. 00002142-201009000-00002 [pii]. 10.1097/RMR.0b013e31823ccebc [PubMed: 22129641]
88. Du J, Takahashi AM, Bae WC, Chung CB, Bydder GM. Dual inversion recovery, ultrashort echo time (DIR UTE) imaging: creating high contrast for short-T(2) species. Magn Reson Med. 2010; 63(2):447–455. Epub 2010/01/26. 10.1002/mrm.22257 [PubMed: 20099332]
89. Williams A, Qian Y, Chu CR. UTE-T2 * mapping of human articular cartilage in vivo: a repeatability assessment. Osteoarthritis Cartilage. 2011; 19(1):84–88. Epub 2010/11/03. S1063-4584(10)00359-6 [pii]. 10.1016/j.joca.2010.10.018 [PubMed: 21035556]
90. Du J, Carl M, Diaz E, Takahashi A, Han E, Szeverenyi NM, et al. Ultrashort TE T1rho (UTE T1rho) imaging of the Achilles tendon and meniscus. Magn Reson Med. 2010; 64(3):834–842. Epub 2010/06/11. 10.1002/mrm.22474 [PubMed: 20535810]
91. Trattnig S, Winalski CS, Marlovits S, Jurvelin JS, Welsch G, Potter HG. Magnetic Resonance Imaging of Cartilage Repair: A Review. Cartilage. 2011; 2(1):5–26.10.1177/1947603509360209

92. Marlovits S, Singer P, Zeller P, Mandl I, Haller J, Trattnig S. Magnetic resonance observation of cartilage repair tissue (MOCART) for the evaluation of autologous chondrocyte transplantation: determination of interobserver variability and correlation to clinical outcome after 2 years. Eur J Radiol. 2006; 57(1):16–23. Epub 2005/10/06. 10.1016/j.ejrad.2005.08.007 [PubMed: 16203119]

93. Mithoefer K, Williams RJ 3rd, Warren RF, Potter HG, Spock CR, Jones EC, et al. Chondral resurfacing of articular cartilage defects in the knee with the microfracture technique. Surgical technique. J Bone Joint Surg Am. 2006; 88(Suppl 1 Pt 2):294–304. Epub 2006/09/05. 88/1_suppl_2/294 [pii]. 10.2106/JBJS.F.00292 [PubMed: 16951101]

94. Welsch GH, Trattnig S, Domayer S, Marlovits S, White LM, Mamisch TC. Multimodal approach in the use of clinical scoring, morphological MRI and biochemical T2-mapping and diffusion-weighted imaging in their ability to assess differences between cartilage repair tissue after microfracture therapy and matrix-associated autologous chondrocyte transplantation: a pilot study. Osteoarthritis Cartilage. 2009; 17(9):1219–1227. Epub 2009/05/05. S1063-4584(09)00095-8 [pii]. 10.1016/j.joca.2009.03.018 [PubMed: 19409295]

95. Mamisch TC, Trattnig S, Quirbach S, Marlovits S, White LM, Welsch GH. Quantitative T2 mapping of knee cartilage: differentiation of healthy control cartilage and cartilage repair tissue in the knee with unloading--initial results. Radiology. 2010; 254(3):818–826. Epub 2010/02/04. radiol.09090335 [pii]. 10.1148/radiol.09090335 [PubMed: 20123898]

96. Holtzman DJ, Theologis AA, Carballido-Gamio J, Majumdar S, Li X, Benjamin C. T(1rho) and T(2) quantitative magnetic resonance imaging analysis of cartilage regeneration following microfracture and mosaicplasty cartilage resurfacing procedures. J Magn Reson Imaging. 2010; 32(4):914–923. Epub 2010/10/01. 10.1002/jmri.22300 [PubMed: 20882622]

97. Crawford DC, Heveran CM, Cannon WD Jr, Foo LF, Potter HG. An autologous cartilage tissue implant NeoCart for treatment of grade III chondral injury to the distal femur: prospective clinical safety trial at 2 years. Am J Sports Med. 2009; 37(7):1334–1343. Epub 2009/05/19. 0363546509333011 [pii]. 10.1177/0363546509333011 [PubMed: 19448048]

98. Saldanha KJ, Doan RP, Ainslie KM, Desai TA, Majumdar S. Micrometer-sized iron oxide particle labeling of mesenchymal stem cells for magnetic resonance imaging-based monitoring of cartilage tissue engineering. Magn Reson Imaging. 2011; 29(1):40–49. Epub 2010/09/25. S0730-725X(10)00222-5 [pii]. 10.1016/j.mri.2010.07.015 [PubMed: 20863643]

99. Majumdar S, Li X, Blumenkrantz G, Saldanha K, Ma CB, Kim H, et al. MR imaging and early cartilage degeneration and strategies for monitoring regeneration. J Musculoskelet Neuronal Interact. 2006; 6(4):382–384. Epub 2006/12/23. [PubMed: 17185834]

100. van Buul GM, Kotek G, Wielopolski PA, Farrell E, Bos PK, Weinans H, et al. Clinically translatable cell tracking and quantification by MRI in cartilage repair using superparamagnetic iron oxides. PLoS One. 2011; 6(2):e17001. Epub 2011/03/05. 10.1371/journal.pone.0017001 [PubMed: 21373640]

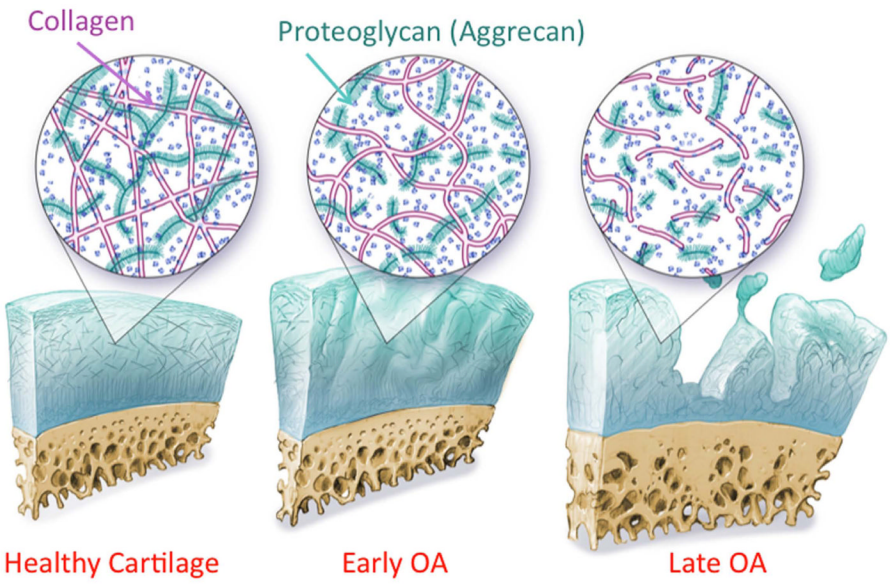

Fig. 1.

Articular cartilage and degeneration during osteoarthritis (OA). Changes at early stages of OA include hydration, loss of proteoglycan, thinning and disruption of collagen. Changes in late stages include further loss of proteoglycan and collagen, dehydration, extensive fibrillation and cartilage thinning, and eventually denudation of the subchondral bone.

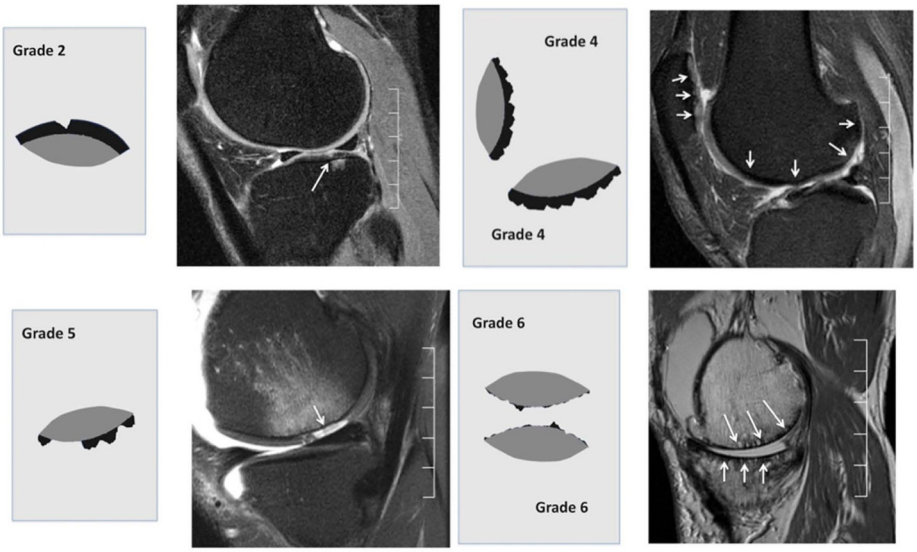

Fig. 2.
Representative MR images with different stages of cartilage lesions and the corresponding WORMS scores.

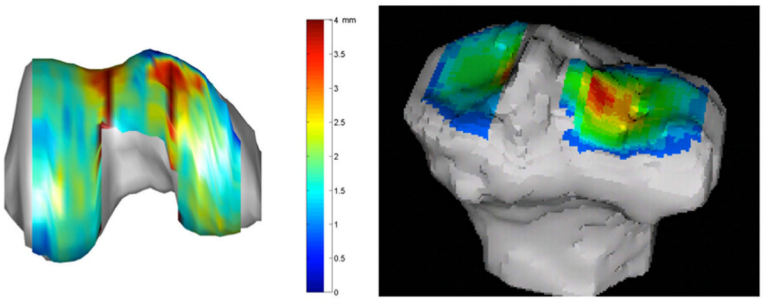

Fig. 3.
Cartilage thickness maps of the knee cartilage overlaying over the femur (left) and tibia (right) respectively.

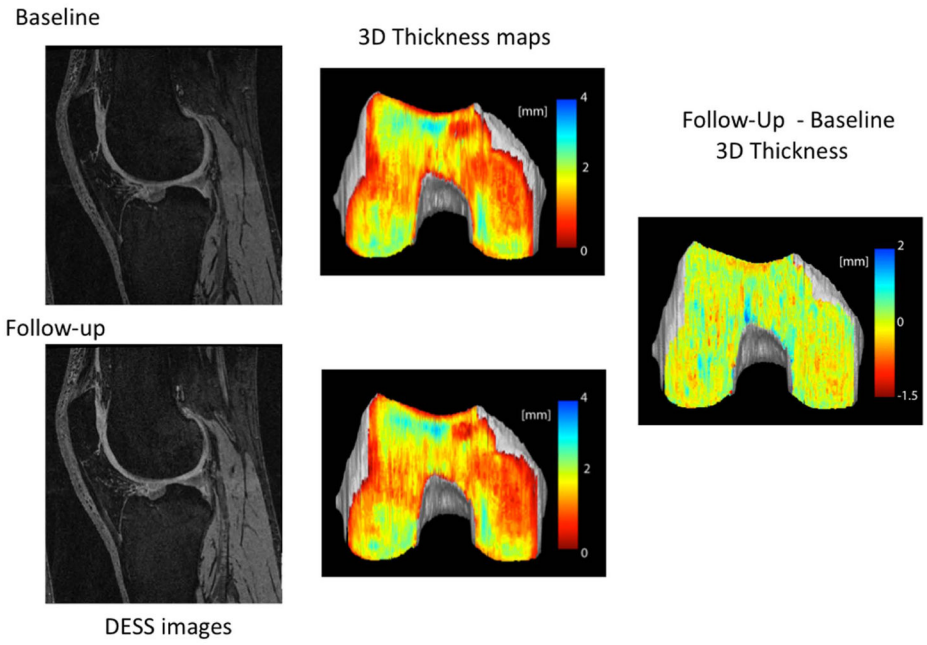

Fig. 4.

An example of intra-subject longitudinal cartilage thickness matching using the technique described by Carballido-Gamio et al (11). DESS: dual echo steady state.

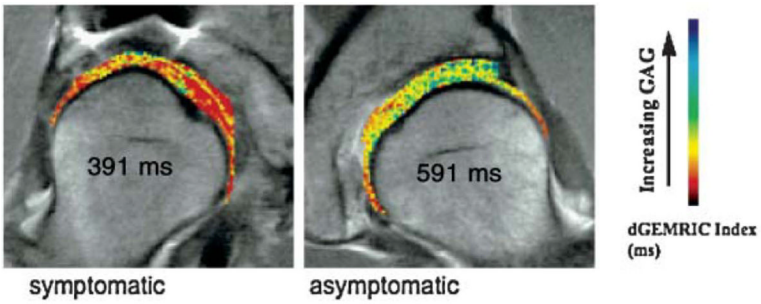

Fig. 5.
dGEMRIC images of the hips of a patient with unilateral hip dysplasia. The symptomatic hip has a much lower dGEMRIC index. Numbers in the images refer to the average dGEMRIC index for the region shown in color. (Figure reprint from reference (29), with permission).

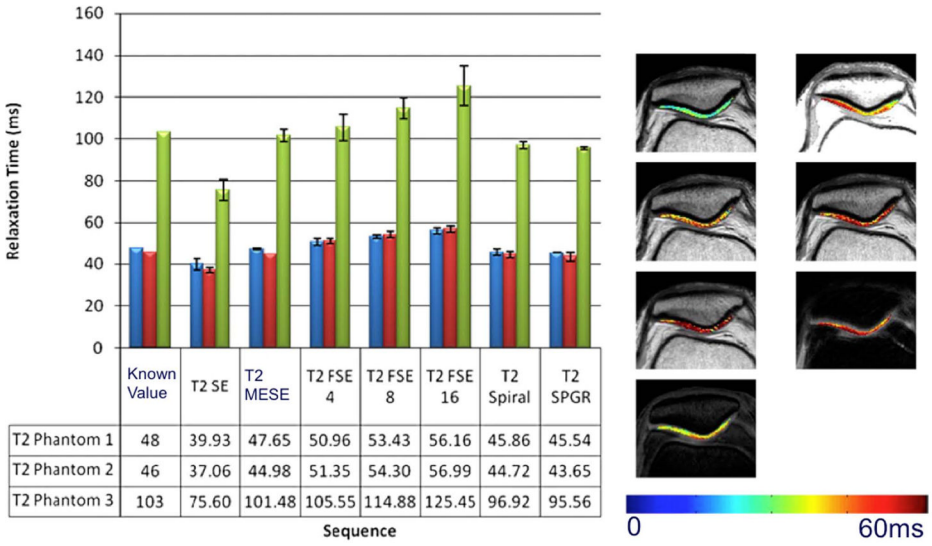

Fig. 6.

Variation of T_2 quantification was observed using different sequences in phantoms (left) and *in vivo* knees (right) (30). SE: spin-echo; FSE-4: fast spin-echo (FSE) with echo train length (ETL) as 4; FSE-8: FSE with ETL as 8; FSE-16: FSE with ETL as 16; MESE: multi-echo spin-echo; SGPR: spoiled gradient echo acquisition.

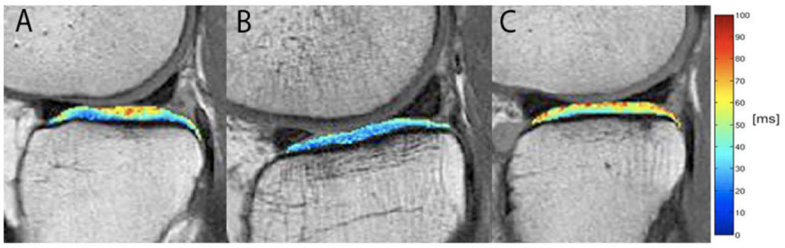

Fig. 7.

T_2 maps of a sedentary subject (A), a light exerciser (B), and a moderate/strenuous exerciser (C) from the OAI cohort with risk factors for knee OA. In subjects with risk factors for knee OA from OAI cohort, light exercisers had lower T_2 values compared with both sedentary and moderate/strenuous exercisers (48), suggesting that there could be a "U" shape of the effect of exercise to cartilage biochemistry.

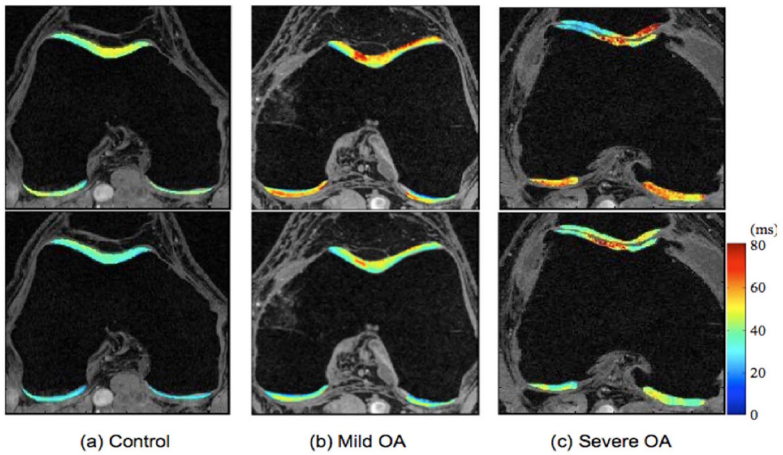

Fig. 8.

$T_{1\rho}$ and T_2 maps of a healthy control (a), a subject with mild OA (b) and a subject with severe OA (c). Significant elevation of $T_{1\rho}$ and T_2 values were observed in subjects with OA. $T_{1\rho}$ and T_2 elevation had different spatial distribution and may provide complementary information associated with the cartilage degeneration.

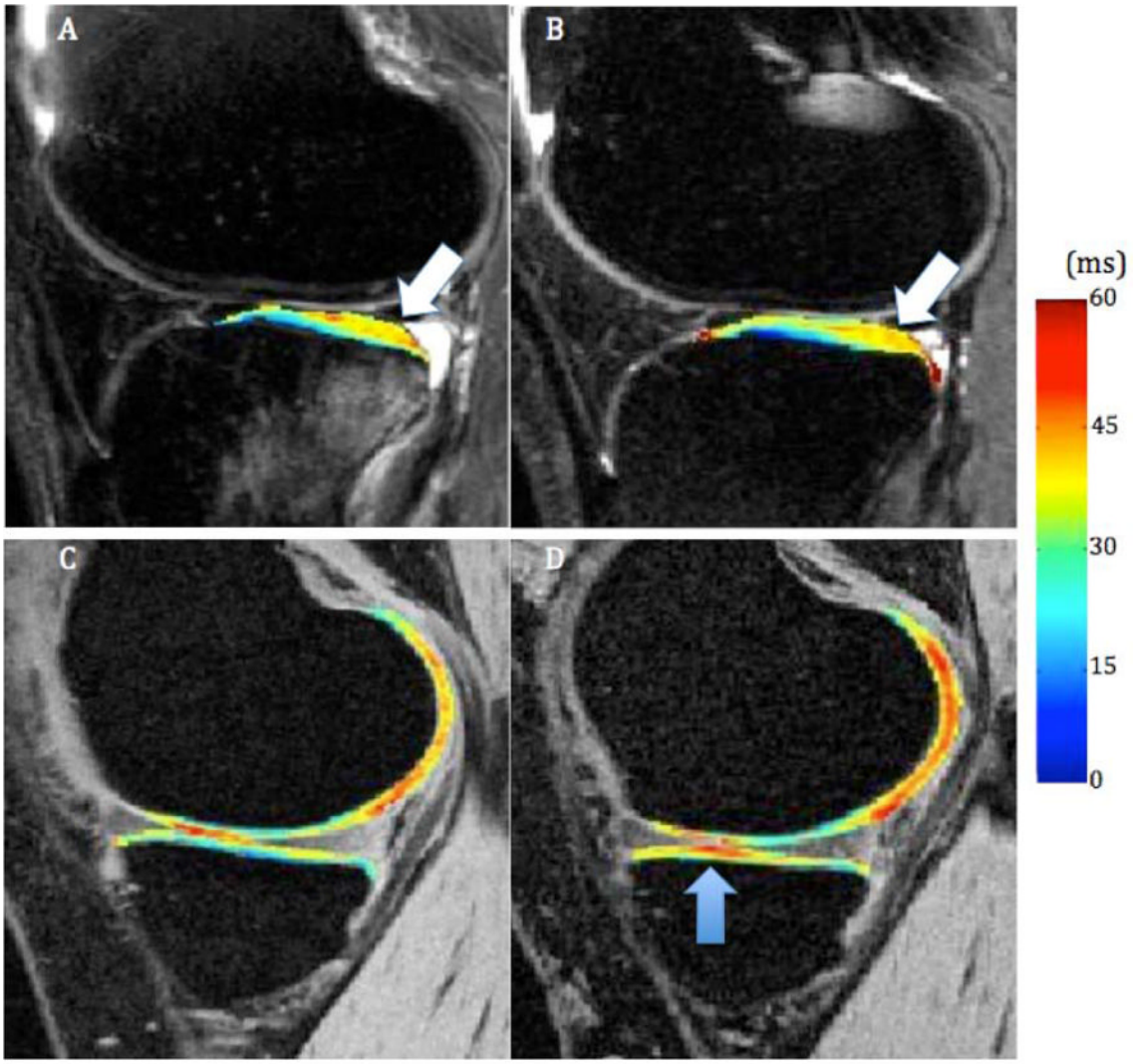

Fig. 9.

$T_{1\rho}$ maps of the lateral side (A and B) and medial side (C and D) of an ACL-injured knee at baseline (A and C) and one-year follow up (B and D) (65). $T_{1\rho}$ values in lateral-posterior tibial cartilage (the region overlying bone bruises, white arrows) were elevated significantly in ACL-injured knees at baseline and remained high at one-year follow despite resolution of bone bruise in lateral tibia. $T_{1\rho}$ values in the contacting area of medial femoral condyle and medial tibia (blue arrow) were significantly elevated in ACL-injured knees at one-year follow up.

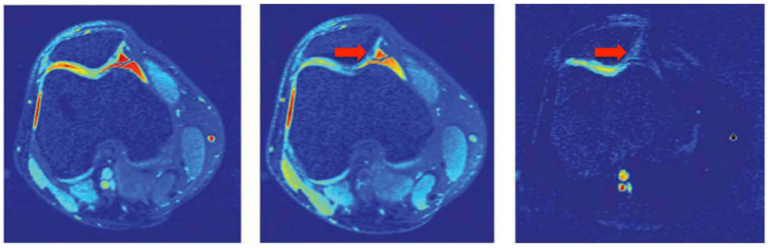

Fig. 10.
gagCEST images of a human patella *in vivo* with irradiation at δ = −1.0 ppm (left), δ = +1.0 ppm (middle), and the difference image (right), displaying a clear demarcation of a cartilage lesion and GAG loss on the medial facet (indicated by arrows) (Figure reprint from reference (73), with permission).

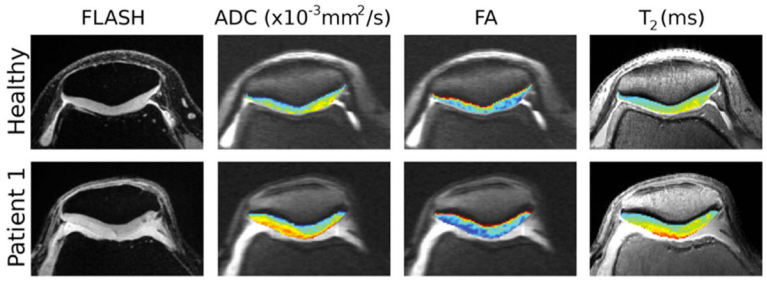

Fig. 11.

High-spatial-resolution morphologic MR images and MR imaging parameter maps (ADC, FA, and T2) in healthy volunteer (top row: 31-year-old man, right knee) and a subject with OA (bottom row: 60-year-old woman, Kellgren-Lawrence grade of 3) (Figure reprint from reference (79), with permission).

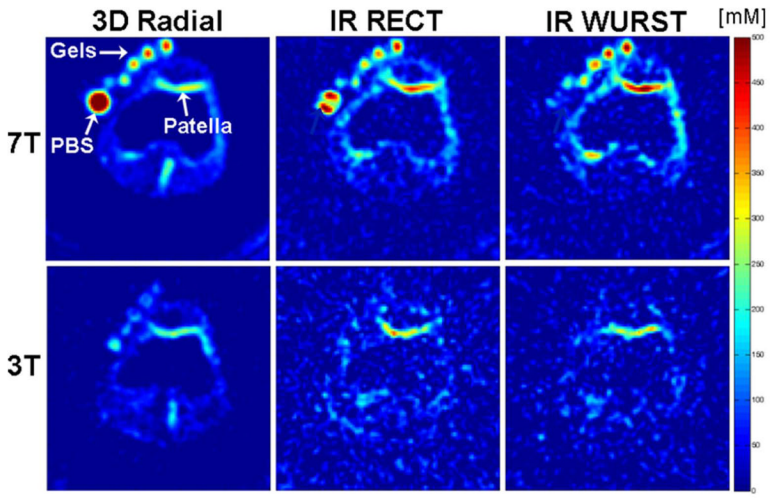

Fig. 12.

In vivo sodium imaging at 7T and 3T respectively. 3T: 15000 projections, RF 80°/0.5 ms, TR 80 ms, 2mm isotropic resolution, time of acquisition (TA) 20 min; 7T: 10000 projections, RF 90°/0.5 ms, TR 100 ms, 2mm isotropic resolution, TA 17 min. IR RECT: 3D radial with the rectangular inversion; IR WURST: 3D radial with the adiabatic Wide-band Uniform Rate and Smooth Truncation (WURST) inversion pulse ("IR WURST" experiment). Images Courtesy of Dr. Ravinder Regatte.

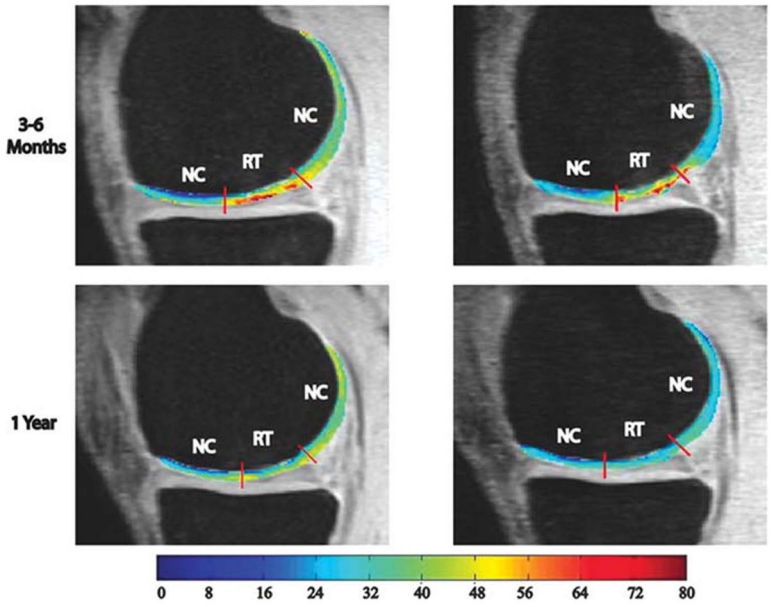

Fig. 13.

Representative $T_{1\rho}$ (left) and T_2 (right) maps 3–6 months and 1-year after microfracture (96). RT: repaired tissue; NC: normal cartilage.